Available online at www.sciencedirect.com

SCIENCE DIRECT®

Lithos 83 (2005) 229–254

LITHOS

www.elsevier.com/locate/lithos

Geochemistry of cumulates from the Bjerkreim–Sokndal layered intrusion (S. Norway). Part I: Constraints from major elements on the mechanism of cumulate formation and on the jotunite liquid line of descent

J.C. Duchesne*, B. Charlier

Department of Geology, Bat B20, University of Liège, B 4000 Sart Tilman, Belgium

Received 11 February 2004; accepted 18 February 2005
Available online 26 April 2005

Abstract

Whole-rock major element compositions are investigated in 99 cumulates from the Proterozoic Bjerkreim–Sokndal layered intrusion (Rogaland Anorthosite Province, SW Norway), which results from the crystallization of a jotunite (Fe–Ti–P-rich hypersthene monzodiorite) parental magma. The scattering of cumulate compositions covers three types of cumulates: (1) ilmenite–leuconorite with plagioclase, ilmenite and Ca-poor pyroxene as cumulus minerals, (2) magnetite–leuconorite with the same minerals plus magnetite, and (3) gabbronorite made up of plagioclase, Ca-poor and Ca-rich pyroxenes, ilmenite, Ti-magnetite and apatite. Each type of cumulate displays a linear trend in variation diagrams. One pole of the linear trends is represented by plagioclase, and the other by a mixture of the mafic minerals in constant proportion. The mafic minerals were not sorted during cumulate formation though they display large density differences. This suggests that crystal settling did not operate during cumulate formation, and that in situ crystallization with variable nucleation rate for plagioclase was the dominant formation mechanism. The trapped liquid fraction of the cumulate plays a negligible role for the cumulate major element composition. Each linear trend is a locus for the cotectic composition of the cumulates. This property permits reconstruction by graphical mass balance calculation of the first two stages of the liquid line of descent, starting from a primitive jotunite, the Tjörn parental magma. Another type of cumulate, called jotunite cumulate and defined by the mineral association from the Transition Zone of the intrusion, has to be subtracted to simulate the most evolved part of the liquid line of descent. The proposed model demonstrates that average cumulate compositions represent cotectic compositions when the number of samples is large (> 40). The model, however, does not account for the K_2O evolution, suggesting that the system was open to contamination by roof melts. The liquid line of descent corresponding to the Bjerkreim–Sokndal cumulates differs slightly from that obtained for jotunitic dykes in that the most Ti-, P- and Fe-rich melts (evolved jotunite) are lacking. The constant composition of the mafic poles during intervals where cryptic layering is conspicuous is explained by a

* Corresponding author. Tel.: +32 43 66 22 55; fax: +32 43 66 2921.
E-mail address: jc.duchesne@ulg.ac.be (J.C. Duchesne).

0024-4937/$ - see front matter
doi:10.1016/j.lithos.2005.03.004

compositional balance between the Fe–Ti oxide minerals, which decrease in Fe content in favour of Ti, and the pyroxenes which increase in Fe.

Keywords: Layered intrusions; Cumulates; Jotunite; Bjerkreim–Sokndal; Rogaland Anorthosite Province; Anorthosite

1. Introduction

Cumulates are central to any petrogenetic discussion on the nature and evolution of magmas. Crystal settling, sorting and accumulation were first invoked by Bowen (1928) to explain differentiation of magmas and the variety of rock types which are generated. Processes of formation of these cumulates in layered intrusions and particularly the origin of layering have then been thoroughly debated. Following Wager and Brown (1968), key contributions on the subject were published in Parsons (1987) and in Cawthorn (1996). Little attention, however, was paid to the whole-rock geochemistry of cumulates compared to rocks assumed to represent liquids (chilled rocks, glass, aphyric rocks). In cumulates, interest was logically focussed on the composition of the cumulus phases in order to define differentiation indices rather than on bulk compositions likely to strongly depend on sorting effects. The use of whole-rock compositions was in general restricted to estimation of the overall composition of the intrusion, such as in the Skaergaard (Wager and Brown, 1968) or Kiglapait (Morse, 1981) intrusions. Other studies using incompatible trace element bulk compositions were aiming at determining the composition, abundance and role of trapped liquid (e.g. Henderson, 1968; Bédard, 1994; Maier and Barnes, 1998).

Here we present the whole-rock major element composition of a collection of cumulates from the large Bjerkreim–Sokndal layered intrusion in S. Norway. It turns out that the compositional variation of bulk cumulates is not chaotic at all, but displays straightforward, simple linear relationships. This observation leads to the concept of two-pole cumulates, the first pole being plagioclase and the second the bulk of the mafic minerals. Factors controlling the bulk composition of these cumulates are discussed in order to bring new constraints on the process of cumulate formation. Our approach also permits determination of cotectic assemblages and, starting from the parental magma composition, to outline a possible liquid line of descent (LLD) for the Bjerkreim–Sokndal intrusion. We also compare it with an LLD reconstructed on the basis of dyke rocks (Duchesne et al., 1989; Vander Auwera et al., 1998).

2. The Bjerkreim–Sokndal layered intrusion

The Bjerkreim–Sokndal layered intrusion (BKSK; Michot, 1960, 1965; Wilson et al., 1996; Duchesne, 2001) is situated in the Rogaland Anorthosite Province, southwest Norway (Fig. 1). This Province comprises units of the AMC suite (Anorthosite–Mangerite–Charnockite) (Fig. 1a): three massif-type anorthosites (Egersund-Ogna, Håland-Helleren and Åna-Sira), two leuconoritic massifs (Hidra and Garsaknatt), jotunite (=Fe–Ti–P-rich hypersthene monzodiorite) dykes (Duchesne et al., 1989) and BKSK. The igneous rocks intruded Sveconorwegian gneisses in the period 930–920 Ma (Schärer et al., 1996) in a post-collisional regime (Duchesne et al., 1999). BKSK covers about 230 km^2 and consists of three lobes (Fig. 1b): the Bjerkreim, Sokndal and Mydland lobes. The rocks display typical textural characteristics of cumulates: igneous lamination and various types of layering, including modally graded layers (Fig. 2). The intrusion is folded in a syncline structure. This results from a gravity-induced subsidence, possibly in response to the diapiric uprise of the surrounding anorthosites (Paludan et al., 1994; Bolle et al., 2000, 2002). This deformation has induced recrystallization of the cumulus minerals, mainly of the plagioclase (Fig. 3).

The BKSK succession of rocks (>7000 m) is vertically subdivided into two parts: a lower part, called the "Layered Series", consisting of anortho-

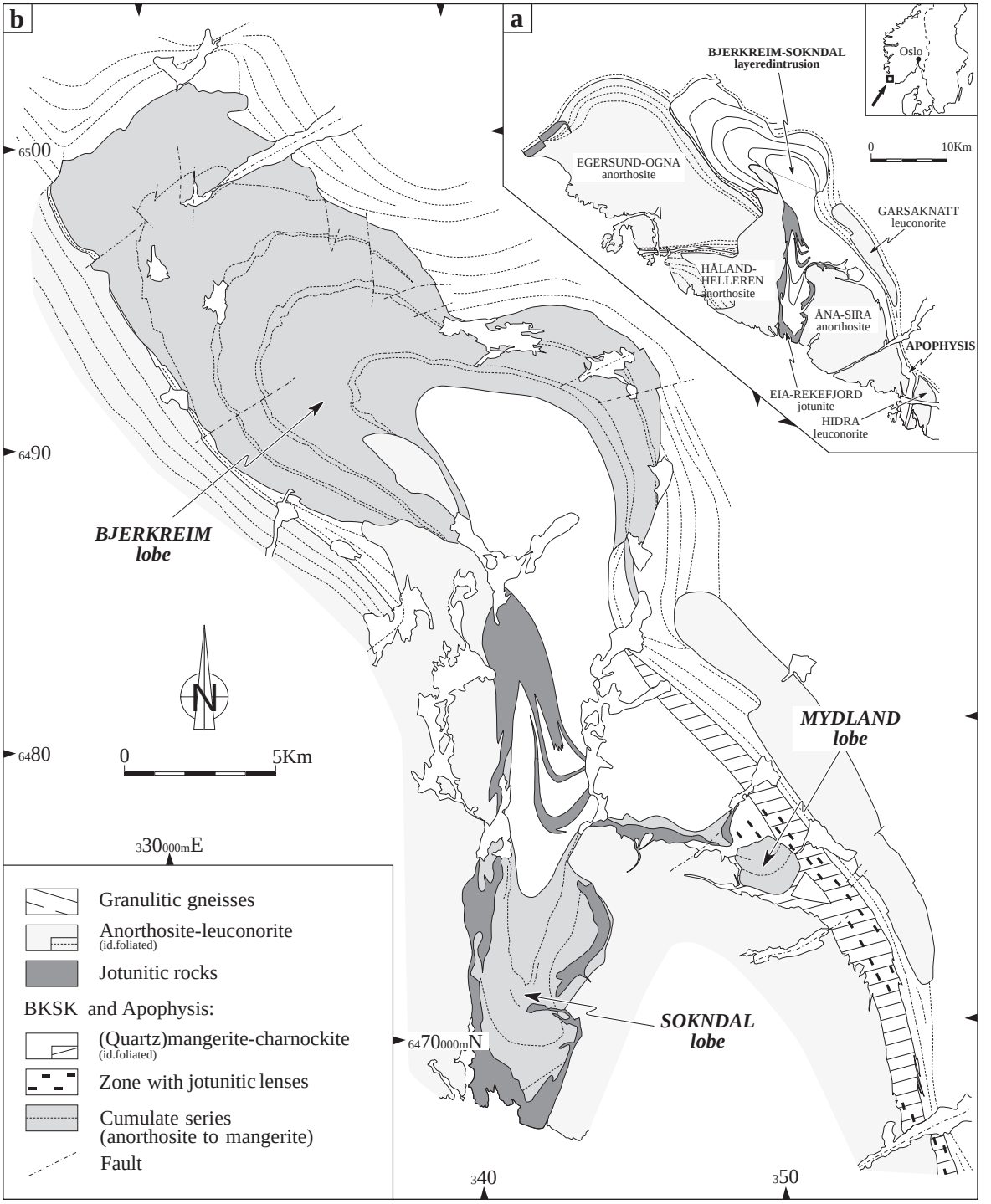

Fig. 1. (a) Schematic map of the Rogaland Anorthosite Province showing the various geological units. (b) The Bjerkreim–Sokndal layered intrusion after Bolle et al. (2000).

sitic, troctolitic, noritic, gabbronoritic, jotunitic and mangeritic cumulates, and an upper part, more massive, formed by liquids of quartz mangerite and charnockite compositions (Duchesne and Wilmart, 1997). In the Bjerkreim lobe (Fig. 4), the sequence of cumulates is subdivided into megacyclic units (MCU IA, IB, II, III and IV), which result from separated magma influxes (Duchesne, 1972a; Jensen et al., 1993; Wilson et al., 1996; Barling et al., 2000). Homogeneous layers up to hundreds of meters thick are typical of the lower and medium parts of the megacyclic units; modally graded layers are conspicuous in the upper parts of MVU III and IV (Fig. 2). The stratigraphic evolution of the cumulates, expressed with the nomenclature of Irvine (1982), is summarized in Fig. 4 (Wilson et al., 1996). Plagioclase is the first mineral to crystallize and is followed successively by ilmenite, Ca-poor pyroxene, magnetite, and apatite together with Ca-rich pyroxene (Table 1). Olivine is present at only two horizons, near the base of MCU III and IV. Isotopic ratio variations provide evidence for continuous contamination by surrounding gneissic rocks (Nielsen et al., 1996). The BKSK parental magma has the composition of a jotunite (see below Table 4) and is very well constrained by the presence of fine-grained chilled rocks at the margins of the intrusion, particularly at a locality called Tjörn (Duchesne and Hertogen, 1988; Robins et al., 1997). Experimental works on the Tjörn composition (Vander Auwera and Longhi, 1994) have confirmed that, at ca. 5 kbar, a magma slightly more magnesian and more calcic than the Tjörn magma crystallizes at the liquidus the same minerals with the same compositions as those developed in the cumulate succession.

Fig. 2. Modally graded layers associated with homogeneous layers. Top of the cumulate pile on the right. Hammer is 30 cm long. Near Storeknuten.

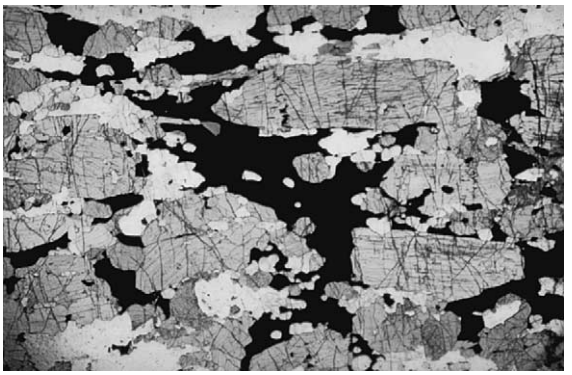

Fig. 3. Microphoto of a gabbronoritic cumulate (phimca-C). Subhedral pyroxenes and smaller apatite define an igneous lamination. Original cumulus plagioclases have been completely granulated (polygonisation). Originally cumulus Fe–Ti oxide minerals have developed an interstitial structure, between the pyroxenes and the granulated plagioclase. Sample 64-44. Transmitted light (ppl). Length of the photo=8 mm.

BKSK and the neighbouring anorthosite intrusions are crosscut by large dykes of rocks of the jotunite kindred (Fig. 5). They vary in composition from dyke to dyke or along the same dyke from jotunite to charnockite (Duchesne et al., 1985, 1989). These dyke rocks and particularly chilled facies have permitted reconstruction of the jotunite LLD (Wilmart et al., 1989; Vander Auwera et al., 1998). Geochemical modelling using chilled melts and cumulus mineral compositions from BKSK have demonstrated that fractional crystallization is a consistent mechanism of differentiation (Wilmart et al., 1989; Vander Auwera et al., 1998). Experimental data have confirmed this modelling (Vander Auwera and Longhi, 1994; Vander Auwera et al., 1998), giving strong support to the hypothesis that BKSK cumulates are conjugated to dyke melts.

3. Sampling and methodology

Samples have been collected in the Layered Series of the Bjerkreim lobe (Fig. 5). The locations of the samples are given in NTU coordinates in Table 2 and are displayed in Fig. 5. They comprise

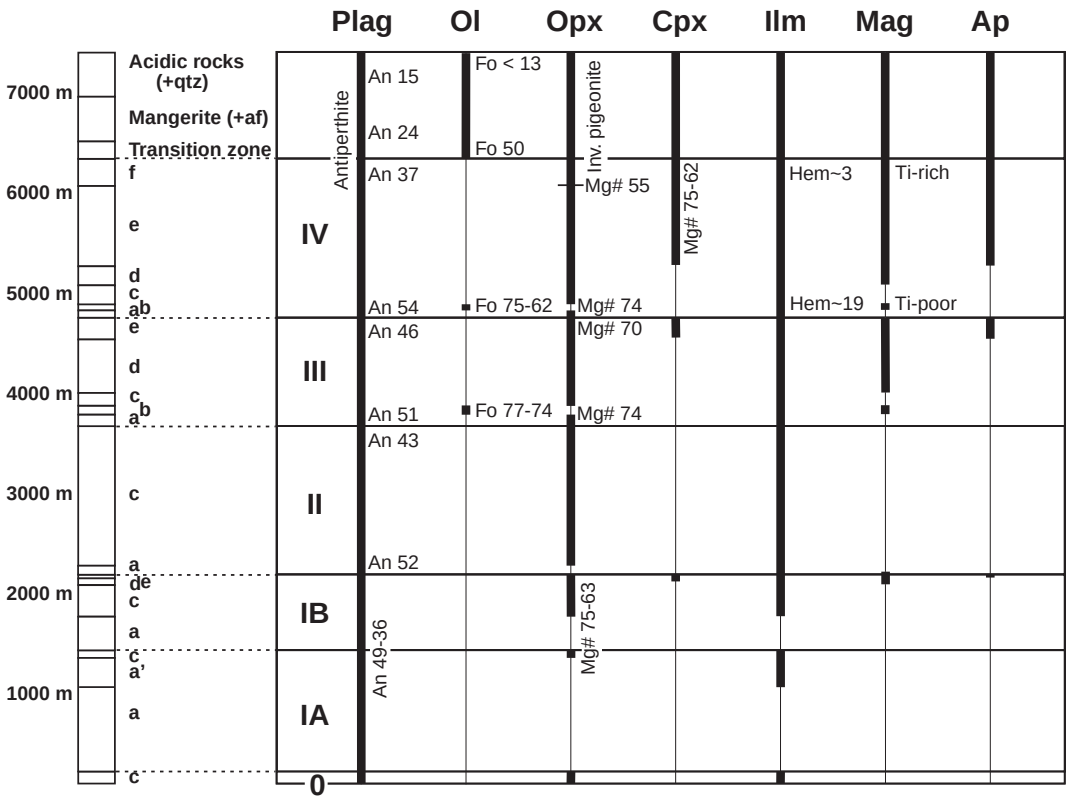

Fig. 4. Generalised stratigraphy of the Bjerkreim–Sokndal Layered Series as developed in the northern part of the intrusion along the axial zone of the syncline (after Wilson et al., 1996). The lower case (a, b, c, d, e and f) refer to stratigraphic zones that are characterised by different assemblages of cumulus minerals (see Table 1): a: p-C, a′: pi-C, b: poim-C, c: phi-C, d: phim-C, e: phimca-C, f: ph'imca-C. Megacyclic units are numbered in roman figures. Plag: plagioclase, Ol: olivine, Opx: Ca-poor pyroxene, Cpx: Ca-rich pyroxene, Ilm: ilmenite solid solution; Mag: magnetite solid solution; Ap: apatite; af: alkali feldspar; qtz: quartz.

57 rocks from Paul Michot's collection of unpublished analyses and 33 rocks collected by the authors. Nine analyses from Jensen et al. (2003) have also been included in the database. The major element compositions of the 99 samples are given in Table 2 and the analytical methods are briefly

Table 1
Relative proportions of the various cumulate types in MCU II, III and IV (estimated by their thickness, see Fig. 4) and comparison with the number of analyses of each type

Cumulate type[a]	MCU II	MCU III	MCU IV	Total	%		Number of analyses	%
pimo-C		1	1	2	3.9		0	
p-C	1	0.1		1.1	2.1		0	
pi-C				0	0.0		0	
phi-C	18	2	2.5	22.5	43.6	Ilmenite–leuconorite	44	44
phim-C	0	7.5	2.5	10	19.4	Magnetite–leuconorite	14	14
phimac-C+ph'imac-C		2.5	13.5	16	31.0	Gabbronorite	41	41
			Total	51.6	100.0		99	

[a] Following the nomenclature of Irvine (1982): a: apatite; c: Ca-rich pyroxene; h: Ca-poor pyroxene; h′: inverted pigeonite; i: ilmenite; m: magnetite; p: plagioclase; o: olivine.

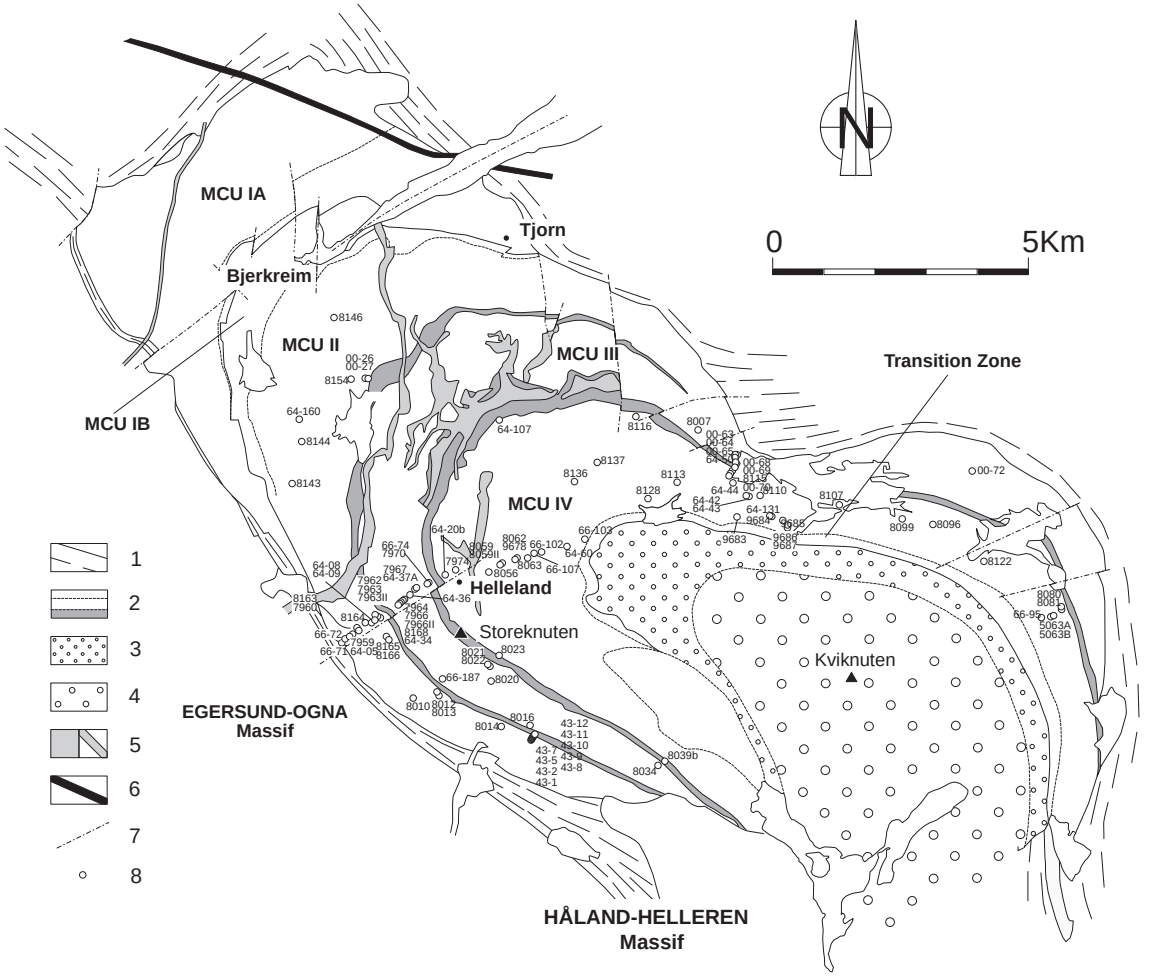

Fig. 5. Northern lobe of the Bjerkreim–Sokndal layered intrusion after Marker et al. (2003). Legend: (1) migmatitic gneisses; (2) cumulate rocks including anorthosite (dashed line indicating upper limit of anorthosite layers) and troctolite layers (shaded); (3) mangerite cumulates; (4) quartz mangerite and charnockite; (5) jotunite dyke and intrusion; (6) dolerite dyke; (7) fault; (8) sample location.

described in Appendix A. The trace elements, measured in 34 samples, will be discussed in a companion paper (Charlier et al., 2005). The samples have been collected from MCU II, III and IV. These MCU display a large variety of cumulates, particularly MCU IV which displays the most complete succession from the most primitive compositions to the most evolved ones—plagioclase composition varies from An_{54} to An_{37} and the Mg# of the Ca-poor pyroxene from 74 to about 62 (Wilson et al., 1996). MCU IA and IB have not been studied because these units are more difficult to sample (the rocks are much coarser-grained and contain abundant plagioclase mega-crysts). Moreover, the plagioclase varies in composition (from An_{49} to An_{39}) with ill-defined correlation with the stratigraphic height.

In MCU II to IV, some particular cumulate types have not been considered. These include monomineralic (anorthosite, ilmenitite, orthopyroxenite) cumulates and ilmenite Ca-poor pyroxene cumulates (hi-C) occurring as rare thin layers near the base of MCU II, III and IV (Fig. 5; Wilson et al., 1996), together with troctolites (pimo-C) present near the base of MCU III and IV. The troctolite formation is linked to magma replenishment episodes (Jensen et al., 1993, 2003). While these lithologies are petrogenetically highly

significant and have been discussed in detail (Jensen et al., 1993, 2003; Wilson et al., 1996), they represent only a very small volume proportion of the whole intrusion (Table 1) and can thus be ignored in the present approach. It can be seen from Table 1 that our sampling is grossly representative of the major cumulate types.

Ultramafic layers and mangeritic rocks cropping out in the the Bakka-Ørsland area (Duchesne et al., 1987) are, however, considered here. They belong to the Transition Zone between gabbronorite at the top of MCU IV and mangerite, and their whole rock compositions are already available (Duchesne et al., 1987). Although it emerges that they do not follow the same rules as the leuconoritic and gabbronoritic cumulates, they play an important role in reconstruction of the LLD.

4. Whole-rock geochemistry: the two-pole cumulate concept

The 99 major element compositions from Table 2 are plotted in classical Harker diagrams in Fig. 6a–b and projected in triangular diagrams in Fig. 7 together with some mineral compositions.

4.1. Three types of cumulates

It emerges from the P_2O_5 and CaO diagrams in Fig. 6a that the whole population can be split into two groups, one comprising gabbronoritic (phimac-C) cumulates and the other comprising the rest of the samples. The latter group can also be separated, particularly on the basis of the TiO_2 diagram, into ilmenite-bearing cumulates (phi-C, here called for short ilmenite–leuconorite), and magnetite-bearing cumulates (phim-C, called magnetite–leuconorite). Logistic regression analysis (Hosmer and Lemeshow, 1989) was used to discriminate between the two leuconorite groups. A stepwise variable selection procedure retained Fe_2O_3, TiO_2, FeO and Na_2O as the most discriminating elements at the 5% critical level ($p<0.05$), the other ones bringing only redundant information. A linear discrimination function based on the four selected elements was derived as follows: $Y=25.1-1.41\ Fe_2O_3+1.73\ TiO_2-1.88\ FeO-3.13\ Na_2O$ and calculated for all 64 samples. Samples with a positive score Y were classified in group 1 (ilmenite–leuconorite) and those with a negative score in group 2 (magnetite–leuconorite). The joint discrimination ability of the 4 selected elements was measured by the proportion of correctly classified samples: only one sample out of 50 from group 1, and 3 samples out of 14 from group 2 were wrongly classified, yielding an overall correct classification rate of 94%.

4.2. The linear trends

A second interesting feature shown by the Harker diagrams is that, in each rock type, the points tend to plot on linear arrays with high correlation coefficients varying from 0.85 to 0.98 (except K_2O, see below) for the leuconoritic groups, and from 0.89 to 0.97 (except CaO and Na_2O, see below) for the gabbronoritic trend (Table 3). In the triangles of Fig. 7, which are projections from the plagioclase (± apatite) compositions, the points definitely cluster into 3 groups. This strongly suggests that the composition of the 3 rock types is a mixture of two end members or poles. In each trend the first pole has the composition of a plagioclase and the second, called here mafic pole, is made up by the sum of all mafic minerals, including apatite.

4.3. The pole compositions

The mafic pole compositions (Table 4) can be accurately identified graphically. The SiO_2 content of the leuconorite mafic poles can be calculated from the regression line of Al_2O_3 vs. SiO_2, assuming 0.7% Al_2O_3 in the ilmenite–leuconorite mafic pole and 0.6% Al_2O_3 in the magnetite–leuconorite (contributed by Ca-poor pyroxenes with 1.5–2.0% Al_2O_3). The deduced values (29.7% and 32.45% SiO_2, respectively) permit calculation of the various element contents with their respective regression lines (Table 3). The calculated compositions are displayed in Table 4. The total to 100 is quite satisfying, if one takes account of loss on ignition.

The plagioclase pole compositions have also been calculated graphically. In the Harker diagrams for FeO, Fe_2O_3, MgO and TiO_2, the lower intercepts of the leuconorite trends (for $y=0$) define the SiO_2 content of the plagioclase poles. For both types, only

Table 2
Major element whole-rock composition and mesoperthite composition (in %) and sample location in the Bjerkreim lobe of BKSK; grid is the EURF89 kilometric UTM grid (32V zone, LK 100 km^2)

Sample	66-71	66-72	64-05	7959	8010	7960	8163	8143	8144	64-160	8146	00-72
Type	phi-C	phi-C	phi-C	phi-C	phi-C	phi-C	phi-C	phi-C	phi-C	phi-C	phi-C	phi-C
MCU	MCU II	MCU II	MCU II	MCU II	MCU II	MCU II	MCU II	MCU II	MCU II	MCU II	MCU II	MCU II
SiO_2	51.42	50.77	48.06	52.56	52.75	46.85	47.32	47.43	50.14	52.12	49.23	49.92
TiO_2	2.84	3.14	4.45	2.19	1.70	5.42	5.46	5.25	1.43	2.45	3.61	3.54
Al_2O_3	22.99	20.65	18.31	22.05	24.10	17.28	17.39	16.95	24.45	24.54	19.95	20.38
Fe_2O_3	2.85	3.13	3.78	1.76	1.85	3.85	3.87	4.47	2.11	2.50	3.33	2.44
FeO	3.05	3.87	6.94	3.52	3.06	8.16	7.57	7.37	2.00	2.44	5.25	5.72
MnO	0.05	0.07	0.09	0.04	0.03	0.10	0.10	0.09	0.01	0.01	0.09	0.08
MgO	2.84	4.97	6.69	3.29	2.89	7.11	7.64	7.66	2.22	1.34	5.64	5.22
CaO	8.63	8.03	6.01	7.84	7.84	5.94	5.79	6.70	10.59	7.85	7.19	7.57
Na_2O	4.27	4.16	4.00	4.89	5.08	3.56	3.62	3.52	6.56	5.60	3.98	4.07
K_2O	0.58	0.42	0.61	0.84	0.88	0.48	0.46	0.50	0.82	0.64	0.64	0.59
P_2O_5	0.04	0.01	0.10	0.06	0.16	0.02	0.04	0.04	0.05	0.11	0.05	0.12
LOI	0.00	0.00	0.46	0.66	0.59	1.16	0.43	0.74	0.42	0.50	0.54	0.98
Total	99.56	99.22	99.50	99.70	100.93	99.93	99.69	100.72	100.80	100.10	99.50	100.63
X	317	318	319	320	329	323	323	309	312	312	319	443
Y	906	907	907	908	895	907	907	938	944	949	967	934

Sample	00-27	43-1	43-2	43-5	43-7	43-8	43-9	43-10	43-11	43-12	8016	66-187
Type	phi-C	phi-C	phi-C	phi-C	phi-C	phi-C	phi-C	phi-C	phi-C	phi-C	phi-C	phi-C
MCU	MCU II	MCU II	MCU II	MCU II	MCU III	MCU III	MCU III	MCU III	MCU III	MCU III	MCU III	MCU III
SiO_2	32.77	50.54	52.81	55.06	53.77	51.76	50.90	52.83	49.71	48.07	50.26	43.45
TiO_2	17.46	3.64	1.95	0.31	0.41	2.53	3.44	1.97	4.24	4.40	2.57	7.38
Al_2O_3	2.19	20.09	23.08	24.97	21.07	21.25	21.50	24.03	21.47	20.28	22.84	13.40
Fe_2O_3	9.91	2.40	1.75	0.84	0.75	1.69	2.39	1.37	2.39	2.11	2.48	6.41
FeO	19.94	5.45	2.95	1.62	4.31	4.65	4.56	2.62	4.91	5.56	3.97	10.71
MnO	0.24	0.08	0.05	0.03	0.07	0.07	0.07	0.04	0.06	0.07	0.06	0.11
MgO	17.19	5.50	3.28	2.14	6.12	4.99	4.43	2.41	3.91	4.44	3.83	11.04
CaO	0.64	7.02	8.19	8.87	7.69	7.74	7.73	8.66	7.72	7.48	7.24	3.96
Na_2O	0.09	4.05	4.69	5.12	4.10	4.20	4.25	4.78	4.26	3.99	5.00	2.24
K_2O	0.05	0.48	0.56	0.60	0.50	0.51	0.50	0.56	0.50	0.46	0.86	0.34
P_2O_5	0.01	0.05	0.07	0.05	0.04	0.05	0.04	0.04	0.04	0.05	0.14	0.01
LOI	0.00	0.47	0.45	0.35	1.12	0.83	0.48	0.72	0.41	2.54	0.56	0.64
Total	100.49	99.77	99.83	99.96	99.95	100.27	100.29	100.03	99.62	99.45	99.81	99.69
X	327	see Jensen et al. (2003)									355	336
Y	956										886	898

Table 2 (*continued*)

Sample	8007	00-64	64-34	64-36	64-37A	00-69	7974	8115	00-65	64-50	66-74	7970
Type	phim-C	phim-C	phim-C	phim-C	phim-C	phim-C	phim-C	phim-C	phimac-C	phimac-C	phimac-C	phimac-C
MCU	MCU III	MCU III	MCU III	MCU III	MCU III	MCU IV	MCU IV	MCU IV	MCU III	MCU III	MCU III	MCU III
SiO_2	48.88	46.77	45.74	48.27	47.41	35.76	52.52	51.35	45.90	35.33	42.58	41.84
TiO_2	3.09	4.72	5.51	3.86	3.82	10.99	2.30	2.75	3.06	6.52	3.76	4.10
Al_2O_3	21.42	17.84	15.51	18.72	17.50	2.27	22.05	21.11	16.93	6.03	14.78	14.61
Fe_2O_3	2.88	4.91	6.34	4.97	5.95	11.94	2.76	2.86	4.05	5.91	5.84	5.62
FeO	4.73	8.63	8.41	6.32	7.76	21.29	3.40	4.35	7.23	18.99	8.65	8.95
MnO	0.07	0.10	0.12	0.09	0.06	0.27	0.05	0.06	0.11	0.24	0.09	0.12
MgO	4.18	6.11	8.24	5.41	5.75	16.35	2.55	4.56	4.97	11.39	5.52	6.34
CaO	7.56	6.35	5.88	6.72	5.96	1.09	7.36	7.50	10.23	9.83	10.20	10.68
Na_2O	4.77	3.70	3.30	4.39	4.02	0.18	5.47	4.52	3.67	1.10	3.84	3.06
K_2O	1.04	0.54	0.31	0.44	0.61	0.04	0.78	0.61	0.73	0.22	0.64	0.42
P_2O_5	0.15	0.10	0.02	0.04	0.12	0.01	0.06	0.15	3.49	4.50	3.23	3.45
LOI	0.67	0.40	0.00	0.00	0.54	0.00	0.56	0.33	0.55	0.00	0.41	0.49
Total	99.44	100.17	99.38	99.23	99.50	100.19	99.86	100.15	100.92	100.06	99.54	99.68
X	392	397	331	331	332	397	341	395	398	398	334	334
Y	944	938	913	913	914	935	918	936	937	937	917	914

Sample	64-42	64-43	8080	8081	8096	8099	8122	8107	8136	8137	00-70	66-95
Type	phimac-C	phimac-C	phimac-C	phimac-C	phimac-C	phimac-C	phimac-C	phimac-C	phimac-C	phimac-C	phimac-C	phimac-C
MCU	MCU IV	MCU IV	MCU IV	MCU IV	MCU IV	MCU IV	MCU IV	MCU IV	MCU IV	MCU IV	MCU IV	MCU IV
SiO_2	48.73	41.92	42.77	44.94	45.69	43.61	44.49	45.37	43.97	44.88	40.42	38.77
TiO_2	2.29	4.33	3.96	3.26	3.22	3.41	4.17	3.75	3.94	3.41	5.15	5.82
Al_2O_3	19.22	11.70	13.07	15.97	15.91	15.99	13.53	16.96	14.17	14.88	9.40	11.63
Fe_2O_3	3.32	6.47	9.30	5.00	5.22	5.91	5.38	5.16	5.37	4.39	6.10	6.82
FeO	5.23	10.66	6.68	8.19	8.33	8.48	10.40	7.47	9.67	9.94	13.18	12.17
MnO	0.08	0.15	0.14	0.10	0.10	0.12	0.20	0.08	0.16	0.18	0.21	0.18
MgO	3.16	7.56	7.06	4.94	5.29	5.34	5.84	4.08	5.85	5.09	10.20	6.88
CaO	9.54	9.28	10.31	9.36	8.69	8.41	8.84	8.98	8.71	8.34	9.97	10.80
Na_2O	4.40	3.54	2.96	4.20	3.56	4.74	3.56	4.66	3.85	4.96	1.94	2.51
K_2O	0.85	0.61	0.62	1.05	0.91	1.29	0.82	0.87	0.80	0.84	0.35	0.41
P_2O_5	1.87	3.33	3.06	2.60	2.22	2.36	2.56	2.03	2.56	2.32	3.96	3.82
LOI	1.03	0.62	0.34	0.44	0.41	0.49	0.33	0.31	0.57	0.43	0.00	0.46
Total	99.72	100.17	100.27	100.05	99.55	100.15	100.12	99.72	99.62	99.66	100.88	100.27
X	399	399	460	460	434	428	443	414	364	370	397	457
Y	931	931	905	905	924	924	914	928	933	937	934	905

(continued on next page)

Table 2 (*continued*)

Sample	8164	8165	8166	8154	7962	7963	7963II	64-08	64-09	8014	8012	8013	00-26
Type	phi-C	phi-C	phi-C	phi-C	phi-C	phi-C	phi-C	phi-C	phi-C	phi-C	phi-C	phi-C	phi-C
MCU	MCU II	MCU II	MCU II	MCU II	MCU II	MCU II	MCU II	MCU II	MCU II	MCU II	MCU II	MCU II	MCU II
SiO_2	48.18	55.24	47.17	47.39	48.40	50.27	50.07	45.77	47.49	48.65	49.57	51.12	53.61
TiO_2	4.55	0.20	5.20	4.97	4.64	3.50	3.28	5.41	4.68	4.25	3.37	2.25	3.49
Al_2O_3	17.39	26.52	18.76	18.11	17.25	17.59	18.99	17.23	17.67	18.56	20.65	23.11	19.35
Fe_2O_3	4.16	0.72	5.18	4.17	2.99	3.48	2.89	5.92	4.38	4.13	2.96	2.57	2.21
FeO	6.77	0.40	6.12	6.47	7.17	5.58	5.91	7.46	7.43	6.42	5.13	3.06	6.04
MnO	0.08	0.01	0.13	0.08	0.08	0.05	0.06	0.07	0.09	0.06	0.05	0.04	0.07
MgO	7.71	0.58	6.81	6.75	7.06	7.40	5.73	7.61	7.36	6.12	4.95	2.94	3.41
CaO	6.14	9.26	6.35	7.08	6.42	6.15	6.77	5.52	5.75	6.17	6.92	7.80	6.46
Na_2O	3.87	5.80	3.75	3.83	3.68	4.40	4.56	3.35	3.64	4.15	4.44	4.96	3.70
K_2O	0.52	0.83	0.47	0.58	0.44	0.64	0.78	0.49	0.47	0.61	0.78	1.02	1.45
P_2O_5	0.03	0.08	0.05	0.06	0.04	0.08	0.12	0.05	0.04	0.06	0.11	0.12	0.07
LOI	0.67	0.69	0.67	0.63	1.74	1.41	1.29	0.52	0.75	0.63	0.67	0.66	0.56
Total	100.07	100.33	100.66	100.12	99.91	100.55	100.45	99.40	99.75	99.81	99.60	99.65	100.42
X	325	331	331	323	325	325	325	324	324	350	334	335	325
Y	910	908	908	957	908	908	908	907	907	888	897	898	957

Sample	00-63	8023	8039b	8116	64-107	64-20b	00-68	7964	7966	7966II	8168	8020	7967
Type	phi-C	phi-C	phi-C	phi-C	phi-C	phi-C	phi-C	phim-C	phim-C	phim-C	phim-C	phim-C	phim-C
MCU	MCU III	MCU IV	MCU IV	MCU IV	MCU IV	MCU IV	MCU IV	MCU III	MCU III	MCU III	MCU III	MCU III	MCU III
SiO_2	45.83	51.75	49.92	51.39	51.33	52.77	55.39	48.54	48.97	49.38	46.44	49.54	40.44
TiO_2	6.45	2.17	1.98	2.44	2.91	2.12	0.88	3.40	3.98	3.64	3.94	3.04	7.92
Al_2O_3	16.23	22.99	20.96	19.86	20.01	19.70	24.44	18.71	15.61	16.19	17.94	19.29	10.70
Fe_2O_3	4.16	2.09	3.56	4.05	2.16	3.18	1.07	4.30	3.84	3.96	5.75	4.50	7.98
FeO	9.57	3.26	5.47	4.38	5.26	4.11	1.70	7.34	9.08	8.77	7.67	6.37	15.01
MnO	0.11	0.05	0.08	0.06	0.08	0.03	0.03	0.04	0.12	0.08	0.09	0.06	0.17
MgO	7.68	3.50	5.07	4.08	6.05	4.06	1.53	5.73	8.19	7.85	6.02	4.88	10.76
CaO	6.01	7.57	6.70	6.73	7.31	7.19	8.34	6.50	5.57	5.45	6.24	6.21	3.82
Na_2O	3.40	4.88	4.31	4.82	4.18	5.19	5.41	4.28	3.48	3.57	4.34	4.51	2.19
K_2O	0.49	0.72	0.93	0.87	0.48	0.83	0.73	0.60	0.42	0.49	0.66	0.69	0.31
P_2O_5	0.16	0.13	0.37	0.39	0.04	0.19	0.09	0.01	0.07	0.03	0.05	0.09	0.06
LOI	0.44	0.58	0.82	0.44	0.28	0.47	0.77	1.25	0.86	0.83	0.37	0.73	0.70
Total	100.53	99.69	100.17	99.51	100.09	99.84	100.38	100.70	100.19	100.24	99.51	99.91	100.06
X	397	348	382	383	347	339	397	331	331	331	331	347	332
Y	938	901	879	947	946	917	935	913	913	913	913	896	914

Table 2 (*continued*)

Sample	8021	8022	8034	5063A	5063B	64-44	8056	8059	8059II	8062	9678	8063	8110
Type	phimac-C	phimac-C	phimac-C	phimac-C	phimac-C	phimac-C	phimac-C	phimac-C	phimac-C	phimac-C	phimac-C	phimac-C	phimac-C
MCU	MCU III	MCU III	MCU III	MCU IV	MCU IV	MCU IV	MCU IV	MCU IV	MCU IV	MCU IV	MCU IV	MCU IV	MCU IV
SiO_2	45.28	35.28	49.46	42.60	44.89	35.46	41.25	34.31	33.46	44.28	43.14	43.53	44.65
TiO_2	3.06	6.71	2.53	4.58	4.14	6.55	4.76	6.71	6.93	3.77	4.05	3.63	4.08
Al_2O_3	15.10	8.66	21.35	12.79	14.26	6.05	13.18	7.63	7.42	14.65	13.29	14.15	15.86
Fe_2O_3	5.66	10.27	2.61	6.12	5.24	9.22	6.10	8.71	9.80	6.67	5.42	5.41	4.88
FeO	8.75	13.62	4.71	9.98	8.98	15.40	10.65	15.78	15.58	8.25	10.63	10.06	8.19
MnO	0.15	0.10	0.05	0.14	0.12	0.24	0.16	0.23	0.24	0.16	0.18	0.16	0.14
MgO	4.08	9.27	4.71	5.23	5.21	11.43	6.40	8.99	9.30	5.70	6.20	7.06	5.14
CaO	9.46	9.19	7.75	10.52	10.26	9.86	9.78	10.05	9.96	8.94	9.43	9.22	9.43
Na_2O	3.99	1.72	0.91	3.12	3.40	1.10	3.22	1.63	1.58	3.81	3.48	3.24	3.87
K_2O	0.94	0.29	0.38	0.49	0.62	0.22	0.58	0.30	0.34	0.72	0.57	0.48	0.82
P_2O_5	2.66	3.41	4.75	3.13	2.68	4.52	3.36	4.79	4.64	2.71	2.48	2.80	2.19
LOI	0.00	0.94	0.31	0.68	0.55	0.00	0.34	0.29	0.39	0.29	0.58	0.40	0.42
Total	99.13	99.46	99.52	99.38	100.35	100.05	99.78	99.42	99.64	99.95	99.45	100.14	99.67
X	347	347	382	458	458	398	347	350	350	353	353	355	401
Y	896	898	879	904	904	933	918	919	919	921	921	921	931

Sample	66-107	64-131	66-102	8113	64-60	8128	9684	9685	9686	9687	9683	66-103	TII
Type	ph'imac-C	ph'imac-C	ph'imac-C	ph'imac-C	ph'imac-C	ph'imac-C	ph'imac-C	ph'imac-C	ph'imac-C	ph'imac-C	ph'imac-C	ph'imac-C	mesoperthite
MCU	MCU IV	MCU IV	MCU IV	MCU IV	MCU IV	MCU IV	MCU IV	MCU IV	MCU IV	MCU IV	MCU IV	MCU IV	
SiO_2	45.00	47.62	43.55	43.50	44.61	46.03	49.08	46.81	44.76	46.43	45.12	42.11	64.18
TiO_2	3.30	2.80	3.80	4.15	3.37	3.09	2.68	3.02	3.64	3.41	2.93	4.05	
Al_2O_3	14.80	15.85	13.02	13.69	13.43	16.17	16.32	15.23	13.57	14.73	14.48	11.67	20.33
Fe_2O_3	6.26	4.19	5.87	7.57	5.86	4.19	3.81	4.42	4.52	3.50	4.55	5.77	
FeO	8.77	9.20	10.69	10.36	10.29	9.79	7.89	9.02	11.12	10.07	11.81	12.23	0.40
MnO	0.12	0.13	0.01	0.18	0.17	0.18	0.15	0.16	0.18	0.18	0.18	0.19	0.01
MgO	5.44	3.86	5.95	6.27	5.46	4.79	3.98	4.94	5.44	5.22	4.76	6.25	0.16
CaO	8.59	7.26	9.19	8.34	8.50	7.57	8.20	8.06	8.48	7.89	7.54	9.29	1.51
Na_2O	4.10	4.32	3.25	3.40	3.92	4.38	4.74	4.28	3.89	3.90	4.51	2.96	5.40
K_2O	0.89	0.97	0.58	0.64	0.83	0.90	1.09	0.92	0.85	0.99	1.25	0.62	7.62
P_2O_5	2.36	1.88	2.78	2.56	2.44	2.29	1.78	2.18	2.51	2.15	2.15	3.02	0.11
LOI	0.47	0.54	0.28	0.30	0.45	0.54	0.42	0.53	0.50	0.78	0.59	0.46	0.5
Total	100.10	98.62	98.97	100.96	99.33	99.92	100.14	99.57	99.46	99.25	99.87	98.62	100.22
X	357	402	358	387	363	380	402	404	404	405	397	367	420
Y	922	926	922	933	922	929	926	925	925	924	925	923	740

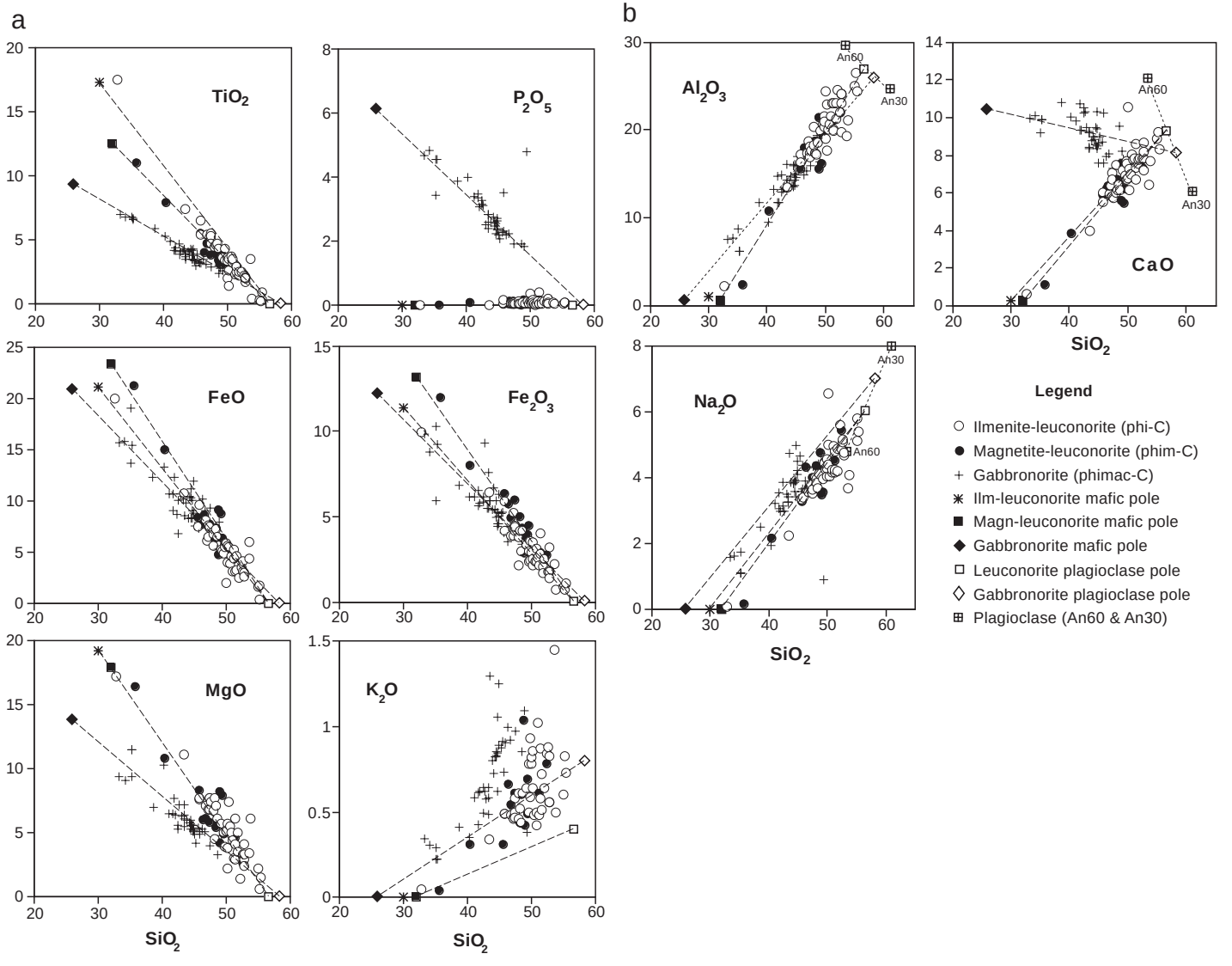

Fig. 6. (a) Harker diagrams. Whole-rock major element compositions plotted against SiO_2. The dashed lines link the plagioclase poles to the mafic poles (see text). (b) Harker diagrams. Plagioclases An_{30} and An_{60} are also plotted to visualise the error on the plagioclase pole compositions (see text).

Table 3
Coefficients a and b in regression lines ($y=ax+b$) and regression coefficient r, with y being an element content and x being the SiO_2 content

	a	b	r
Ilmenite–leuconorite			
TiO_2	−0.69	37.86	0.96
Al_2O_3	0.96	−27.75	0.91
FeOt	−1.15	65.52	0.96
FeO	−0.78	44.26	0.94
Fe_2O_3	−0.41	23.62	0.93
MgO	−0.69	39.81	0.91
CaO	0.35	−10.20	0.85
Na_2O	0.23	−7.04	0.85
K_2O	irrelevant		0.60
P_2O_5	irrelevant		0.22
Magnetite–leuconorite			
TiO_2	−0.53	29.29	0.98
Al_2O_3	1.10	−35.12	0.94
FeOt	−1.50	84.06	0.97
FeO	−1.02	56.35	0.96
Fe_2O_3	−0.54	30.80	0.93
MgO	−0.72	40.96	0.92
CaO	0.36	−10.87	0.92
Na_2O	0.28	−9.38	0.93
K_2O	irrelevant		0.74
P_2O_5	irrelevant		0.41
Gabbronorite			
TiO_2	−0.30	17.08	0.97
Al_2O_3	0.77	−19.43	0.92
FeOt	−0.96	56.66	0.95
FeO	−0.62	36.97	0.85
Fe_2O_3	−0.37	21.88	0.84
MgO	−0.44	25.26	0.89
CaO	irrelevant		0.57
Na_2O	irrelevant		0.71
K_2O	irrelevant		0.72
P_2O_5	−0.16	9.78	0.74

one composition can be defined at the average values (56.6% SiO_2) of the lower intercepts. This value in turn defines the Al_2O_3, CaO and Na_2O values of the plagioclase composition (Table 4), with a good total to 100. The anorthite content of the plagioclase pole is An_{45}. Comparison with the stratigraphic evolution of the plagioclase composition in BKSK (see, for example, Fig. 5 in Wilson et al., 1996) shows that An_{45} is a very good average for the composition of the plagioclase in the leuconorites.

In a similar way, for the gabbronoritic mafic pole, an assumed content of 0.5% Al_2O_3 leads to 26% SiO_2 and, through the regression lines, to TiO_2, FeO, Fe_2O_3, MgO and P_2O_5 values (Table 4). The CaO value is loosely constrained graphically because of a lower r coefficient ($r=0.53$). The dispersion of the points is due to the fact that, here, the mafic pole value for CaO accumulates small fluctuations in the modal proportions of three minerals (viz. plagioclase, Ca-rich pyroxene and apatite) instead of one (plagioclase) in the leuconorites. To make up for this lack of accuracy, we have imposed a value of 8.1% CaO for the plagioclase pole, corresponding to the SiO_2 and Al_2O_3 values of An_{37} (see Table 4). Then passing through the average gabbronoritic composition (43.1% SiO_2 and 9.1% CaO), we obtain 10.4% CaO corresponding to 26% SiO_2 for the mafic pole of the gabbronorite trend. Again the sum to 100 obtained attests the validity of the hypotheses. Moreover, the obtained plagioclase An_{37} value is quite in agreement with the average plagioclase composition observed in the evolution of gabbronorites (Wilson et al., 1996).

The mineralogical composition of the mafic poles can be estimated by least-square calculation using a set of mineral compositions. It can be estimated that the ilmenite–leuconorite mafic pole is made up of 45% hemo-ilmenite + 55% Ca-poor pyroxene, the magnetite–leuconorite of 49% Ca-poor pyroxene + 37% ilmenite and 14% magnetite, and the gabbronoritic mafic pole 40% Ca-poor pyroxene + 9% Ca-rich pyroxene + 14% apatite + 36% Fe–Ti oxides. These proportions can also be grossly evaluated in the triangular plots (Fig. 7).

It is clear that the plagioclase pole composition defined by the present approach is an average value encompassing the range of cryptic variations of the plagioclase. A possible visual estimate of the error (ca. ± 5% An) can be deduced from the CaO, Al_2O_3 and Na_2O Harker diagrams (Fig. 6b). The same remark holds for the mafic pole compositions, which are also affected by an error reflecting the cryptic evolution of the mafics. However, a puzzling mechanism, commented on below, buffers the bulk Mg# evolution and drastically limits the range of variations.

4.4. Influence of the trapped liquid fraction

As already mentioned, some elements show a lower regression coefficient with SiO_2 (Table 3). This is the case for CaO ($r=0.53$) in gabbronoritic type, P_2O_5 ($r=0.29$) and K_2O ($r=0.68$) in leuconoritic type

Table 4
Major element compositions of poles, cumulates and melts in the graphical modelling

	Leuconorite types					Gabbronorite type			Jotunite type			Melts		
	Aver. Ilm–leuco. C1	Aver. Magn–leuco C1+	Mafic pole Ilm–leucon	Mafic pole Mt–leucon	Plag. pole (An_{45})	Aver. Gabnor C2	Mafic pole	Plag. Pole (An_{37})	Mafic pole 3	Feldspar F3 ($An_{32}Or_{12}$)	Cumulate C3	L2 melt	L3 melt	Tjörn[a]
SiO_2	49.81	46.82	29.7	32.45	56.60	43.25	26.00	58.40	26.10	60.00	40.00	50.00	53.30	49.7
TiO_2	3.65	4.63	17.45	12.22		4.05	9.26		10.40		6.20	3.63	3.43	3.63
Al_2O_3	20.01	16.44	0.73	0.6	27.00	13.71	0.50	25.90	0.70	24.00	10.40	12.59	11.85	15.78
Fe_2O_3	3.10	8.83	11.38	13.17		5.77	12.18							
FeO	5.41	5.39	21.09	23.41		10.15	20.85		41.06[b]		24.22[b]	15.34[b]	15.12[b]	12.87[b]
MnO	0.07	0.10	0.24	0.28		0.15	0.32							0.15
MgO	5.30	7.08	19.23	17.53		6.11	13.77		8.12		4.85	3.62	2.50	4.44
CaO	7.04	5.75	0.08	0.65	9.27	9.14	10.4[c]	8.1[c]	9.06	6.66	8.10	6.81	5.52	6.81
Na_2O	4.24	3.71			6.06	3.40		7.00		6.10	3.00	3.18	3.05	3.88
K_2O	0.63	0.53			0.40	0.70		0.80		2.08	0.83	1.61	2.08	1.05
P_2O_5	0.08	0.06				2.91	6.00		3.55		2.08	1.77	1.15	0.64
Total	99.34	99.34	99.90	100.31	99.33	99.34	99.28	100.20	98.99	98.84	99.68	98.55	99.68	99.45

[a] Average of two samples, from Duchesne and Hertogen (1988).
[b] Total Fe as FeO.
[c] Estimated.

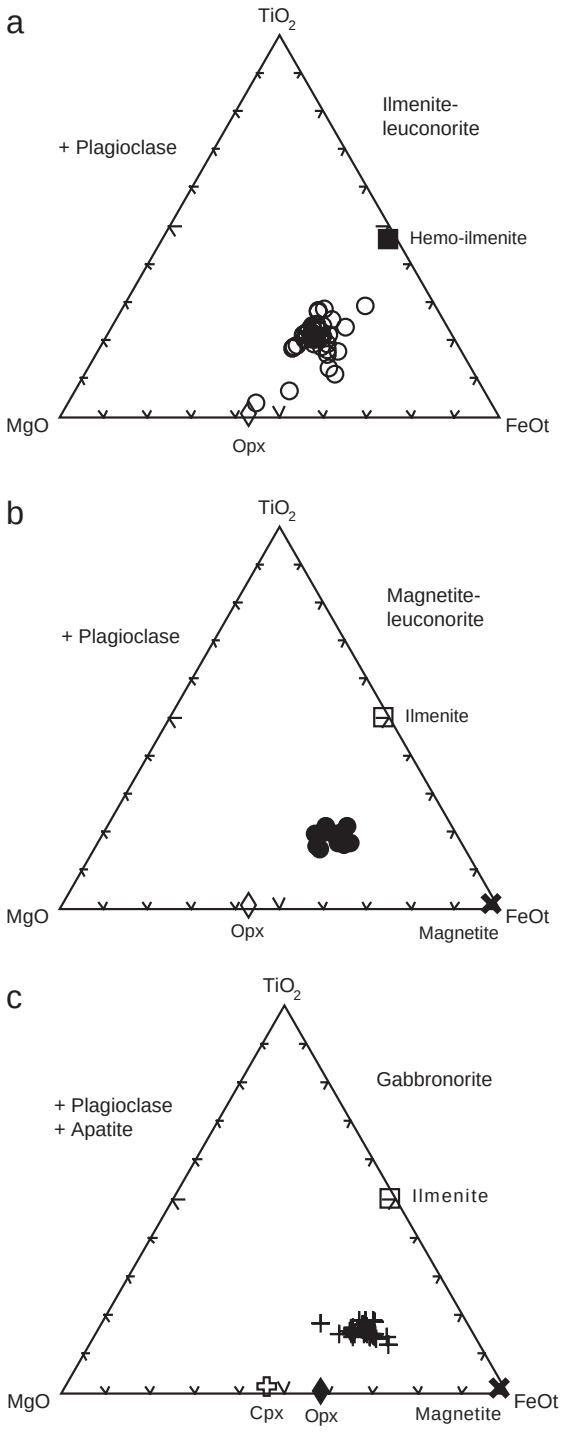

Fig. 7. MgO–TiO_2–FeOt triangular plots of cumulate compositions. (a) Ilmenite–leuconorite cumulate; (b) magnetite–leuconorite cumulate; (c) gabbronorite cumulate. Representative mineral compositions from Duchesne (1972a, 1972b) are also plotted. Note that a slight variation in the Mg# of the mafic pole is clearly visible in each rock type.

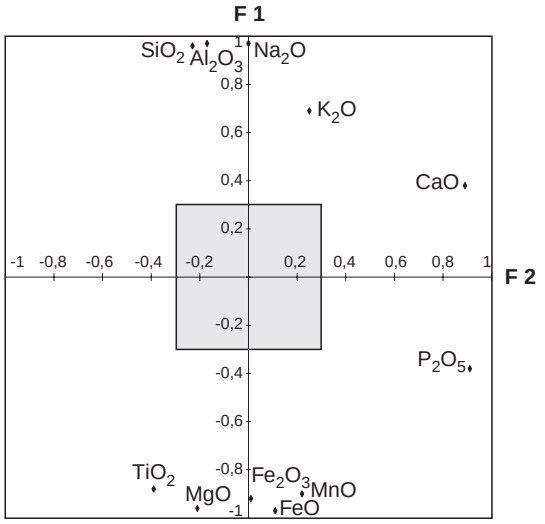

Fig. 8. Graphical representation of the factor loadings in the plane of the principal components F_1 and F_2. The shaded square limits the domain of insignificant values.

(Fig. 6). As already discussed above, the CaO variations are possibly due to the fact that calcium is present in both gabbronorite poles, i.e. in plagioclase and in Ca-rich pyroxene and apatite, thus amplifying the fluctuations of modal proportions and mineral compositions. For P_2O_5 and K_2O, we suggest that the dispersions are mainly due to variation in the intercumulus trapped liquid fraction (TLF). To test this hypothesis we have investigated the leuconoritic rocks by principal component analysis (Davis, 1986). Apatite is not a cumulus phase here and the P_2O_5 content of the rock must therefore result from crystallization of a TLF. Two principal components, F_1 and F_2, account for 71.3% and 8.5% of the total variance, respectively. Fig. 8 shows that F_1 is heavily and positively loaded by Si, Al and Na, representing the plagioclase pole, and negatively loaded by Fe, Mn, Mg, and Ti, representing the mafic pole. F_1 thus measures the contrast between the two poles identified graphically. F_2 is loaded by P and Ca and to a lesser extent by K. Obviously the TLF, containing K_2O

(presumably in very minor K-feldspar) and P_2O_5 (in very minor apatite), can explain 8.5% of the total variance. An elaborated way of calculating the TLF will be developed in a companion paper (Charlier et al., 2005). Here we use a simple graphical approach. Fig. 9 shows the P_2O_5 vs. K_2O relationship in leuconoritic rocks and in the parental magma (Tjörn). Assuming that the TLF has the composition of the parental magma and that the most frequent value represents a TLF-devoid cumulate, it can be calculated that the amount of TLF averages 10%, a relatively low value, close to the limit between adcumulates and mesocumulates (Irvine, 1982), and suggesting that the limit of compaction was the controlling factor (Irvine, 1980). Note that K and Ca are also loading F_1 in Fig. 8, because these elements are constituents of the plagioclase. Ca has however a relatively low loading value on F_1 (0.4) because it also participates in apatite in the mafic pole.

4.5. The two-pole cumulates

In conclusion of the graphical and statistical approaches it is clear that the whole-rock chemistry of the most abundant cumulates in BKSK reveals that the most important cause of variation can be described in terms of mixing between a plagioclase and a mafic pole. In ilmenite–leuconorite, the plagioclase is $An_{45\pm5}$ and the mafic pole is made up of Ca-poor pyroxene and hemo-ilmenite in constant proportions.

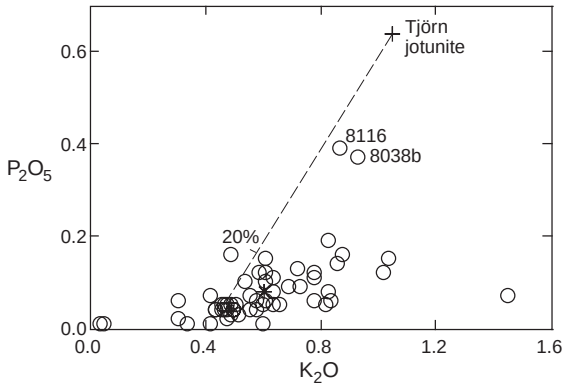

Fig. 9. P_2O_5 vs. K_2O in leuconorite types and in Tjörn parental magma composition. The dashed line ties the Tjörn jotunite composition to the most common cumulate composition. The TLF content rarely exceeds 20%, except in samples 8116 and 8038b.

In magnetite–leuconorite, the same plagioclase coexists with a mafic pole made up of constant proportions of Ca-poor pyroxene, ilmenite and magnetite. In gabbronoritic cumulates, a plagioclase $An_{37\pm5}$ is mixed with a mafic pole containing constant proportions of Ca-poor and Ca-rich pyroxenes, ilmenite, magnetite and apatite. The TLF plays only a minor role in the major element composition and, as a first approximation, can be neglected. In other words, the major factor responsible for the modal layering in BKSK is the variation in modal ratio of plagioclase to the sum of the mafic phases.

Another interesting conclusion that emerges from this approach is that there is no noticeable chemical difference in a given cumulate type between samples coming from different MCU (Table 2): they all plot on the same linear trends. This suggests that the various influxes of magma from MCU II to IV had essentially the same composition.

4.6. An exception to the rule: the Transition Zone (TZ) cumulates

The cumulates constituting the transition from layered gabbronorites (ph'imac-C) of MCU IV to mangeritic cumulates are characterised by the reappearance of olivine which, upwards, remains a permanent mineral in mangerite and in some quartz mangerite and charnockite (Duchesne et al., 1987; Wilson et al., 1996). Olivine rapidly changes in composition in the sequence from Fo_{50} to almost pure fayalite. The feldspar is an antiperthite plagioclase at the base of the TZ, joined further on by mesoperthite which progressively increases in proportion to become the only feldspar in mangerite, quartz mangerite and charnockite. The TZ is relatively thin, amounting only to 30 to 50 m thick in the Bakka-Örsland area (Duchesne et al., 1987). Although small in volume compared to the leuconoritic and gabbronoritic sequences (TZ represents a thickness less than 2% of the total Layered Series in Fig. 4), these rocks play a decisive role in the evolution of the LLD, as will be developed below. Fig. 10 shows that, in these cumulates, a 2-pole relationship does not explain the rock composition for CaO and P_2O_5. The latter element particularly decreases in the mafics by almost a factor 2 from the base (UML1) to the top (UML2) of the Transition Zone. The relationship does not

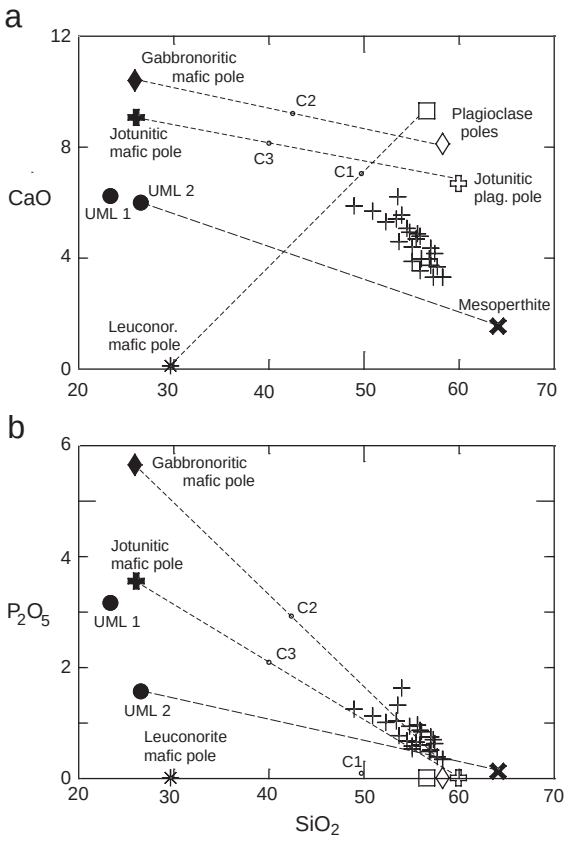

Fig. 10. Transition Zone cumulate composition in Harker diagrams: (a) CaO diagram; (b) P_2O_5 diagram. The leuconoritic, gabbronoritic and jotunitic poles and their respective average cumulate compositions (C_1, C_2 and C_3, respectively) are also represented. UML 1 and 2 refer to ultramafic layer compositions from the base and top of the Transition Zone, respectively. Legend: + (cross): Transition Zone cumulate compositions from Duchesne et al. (1987) and Duchesne and Wilmart (1997). Note that in the CaO vs. SiO_2 diagram, the rock compositions grossly define a straight line in a triangle defined by UML compositions, mesoperthite and a plagioclase, thus suggesting a constant mafic/plagioclase ratio and a variation controlled by the mesoperthite content.

correspond to a simple mixture of two components. Clearly a unique mafic pole cannot be defined for the TZ, and, similarly, the appearance of mesoperthite in the feldspar assemblage and its rapid increase in proportion make irrelevant the definition of a feldspar pole with a fixed composition. Obviously the mechanism of formation is more complex than in the underlying Layered Series and has involved some sorting of minerals. Interestingly, the mafic minerals, represented by UML1 and UML2, show little variation in bulk composition, except for P_2O_5, so it is mainly the variation in feldspar composition and in apatite content that determines the spread of the silica-rich rock composition.

5. Implication for the cumulate formation

The 2-pole cumulate concept, very simple in essence, is quite intriguing. A first feature worth considering is the difference in behaviour between plagioclase and the mafic minerals. One could argue that density is the controlling factor. Indeed plagioclase has a significantly lower density than the other minerals. Moreover, its density (for $An_{45–50}$, $\rho = 2.62–2.63$, Campbell et al., 1978) is lower than the BKSK parental magma density ($\rho = 2.74–2.77$, Vander Auwera and Longhi, 1993), while the other minerals have densities considerably above that of the magma. One could thus see a plagioclase floating or, at most, remaining stagnant in the magma, and mafic minerals settling by gravity, the variation of the settling parameters of the Stoke's law controlling the proportion of the minerals.

5.1. Precluding gravity-controlled crystal sorting

This explanation, however, fails to account for the lack of sorting between the mafic minerals. Indeed all mafic minerals, though of contrasted densities ($\rho_{apatite} = 3.1–3.3$, $\rho_{Ca\text{-}rich\ pyroxene} = 3.3–3.5$, $\rho_{Ca\text{-}poor\ pyroxene} = 3.4–3.7$, $\rho_{ilmenite} = 4.7$, $\rho_{magnetite} = 5.2$; Deer et al., 1966), always remain in the same proportion in a given mafic pole. This feature is hard to explain in a gravity-controlled crystal sorting process, and it strongly suggests that crystal settling was not operating at all. Consistent with this hypothesis is the complete lack of grain-size graded layering in BKSK (Wilson et al., 1996). We are thus compelled to consider that all minerals have grown in situ by heterogeneous nucleation on top of the crystal pile, as first suggested by Campbell (1978) and McBirney and Noyes (1979), and further elaborated by many others (see e.g. Parsons, 1987; Cawthorn, 1996). We thus adopt a model of adcumulus growth "at the topmost layer of cumulus grains in direct contact with the magma" (Sparks et al., 1985). Such a process can explain the relatively

low amount of TLF, though this is not a compelling argument because compaction of the cumulate can also have contributed to the extraction of the TLF.

5.2. Precluding immiscibility

The constant proportion of mafic minerals in a pole also precludes immiscibility of an Fe–Ti-rich liquid in the course of crystallization. This process, forged by Philpotts (1981) and based on the interstitial habit of the opaque minerals, is currently invoked to explain Fe–Ti oxide mineral deposits (see the review by Force, 1991). The evidence here provided by the constant proportion of the Fe–Ti oxide minerals relative to the rest of the mafics is not in favour of the formation of an immiscible Fe–Ti rich liquid at any stage of the crystallization process. Indeed such liquids, with a density between 4.7 and 5.2 in sharp contrast with the silicate melt density, would have segregated and formed very oxide-rich mineral layers, thus modifying the proportion of the mafic minerals. Similarly, no dykes or off-shoots of oxide-rich rocks have ever been observed in BKSK. On the other hand, the interstitial habit of the oxide minerals has found an explanation in subsolidus grain-boundary readjustment (Paludan et al., 1994; Duchesne, 1996).

5.3. Tentative mechanism of cumulate formation

The cause of the variation in the plagioclase proportion of cumulates is another intriguing feature. In the in situ crystallization model, which in the present case is the only viable mechanism since gravity sorting is not operating, the variation in the modal proportions of a cumulate must result from variation in the nucleation rates. It is, therefore, in the concept of oscillatory nucleation (Wager and Brown, 1968; Campbell, 1978; Maaløe, 1978; Morse, 1979) that we must investigate. Though nucleation processes have recently received considerable attention (Hort et al., 1993; Greer et al., 2003), application to layered rocks is still hampered by the chemical complexity of multi-saturated systems.

Solving this problem is outside the purposes of this work, but it is interesting to outline what constraints the simple properties of the BKSK cumulates can bring to models of cumulate formation. In the case of BKSK, the classical view (e.g. Morse, 1979), in which a layer of cumulus minerals results from crystallization of a sheet of supercooled magma, descending from the roof region of the magma chamber and spreading on top of the crystal pile, is not viable. It indeed implies repeated large-scale currents in the magma chamber, and this phenomenon is totally inconsistent with the presence of a zoned magma in the chamber, a characteristic demonstrated for BKSK by Nielsen and Wilson (1991) and accepted by Wilson et al. (1996). We have thus to accept that the zoned magma column has broken into multiple stratified layers by a double-diffusive mechanism, as suggested by McBirney and Noyes (1979) for the Skaergaard intrusion and further elaborated by Irvine (1980). Each layer is "well mixed and separated from the liquid layer above by a sharp interface where a stable step in density and temperature is maintained" (McBirney and Noyes, 1979, p. 543). Theoretically a layer can crystallize completely before the start of the crystallization in the next layer when the decrease of the liquidus temperature of the magma with depth (due to the pressure decrease) is lower than the ΔT step at the interface between the two layers. The thickness of the layers would be controlled by the intensity of the temperature and composition gradients (Irvine, 1980), and thin and numerous layers would thus be expected in the upper parts of the MCU, closer to the roof. In this model, the mafic minerals start crystallizing in equilibrium proportions, i.e. in their relative proportions in the mafic pole of the cotectic assemblage. This implies negligible differences in their nucleation rates. On the other hand plagioclase nucleation is "difficult" (Campbell et al., 1978) and needs a larger degree of supersaturation. Now two cases can be considered: (1) the layers show a constant mode, and thus a constant proportion of plagioclase; (2) the layers are modally graded, with an increase in the plagioclase content upwards (Fig. 2). As already noted, the thickness of constant-mode layers is greater than that of modally graded layers (several meters to decameters vs. tens of centimeters). In both types of layers the grain size remains constant, suggesting that crystal growth rate is not a critical factor. In modally graded layers, the increase in plagioclase content upwards implies an increase in nucleation rate, due to self-nucleation and/or to continuous increase in supersaturation. The latter is likely to occur in a thin layer of magma which cools

rapidly because of a conductive heat loss greater than the latent heat production. The process ends when the whole layer of magma is consolidated. In constant-mode layers, a constant nucleation rate is required, and this can be obtained if the degree of supercooling is kept constant with an equilibrium temperature resulting from the balance between heat loss and heat production, a regime more likely to be attained in thick layers (Brandeis and Jaupart, 1987). Finally, the occurrence of modally graded layers in the upper parts of MCU, at smaller distance from the roof, is consistent with a higher cooling rate, and with thinner layers of magma. In conclusion, the proposed model of in situ crystallization, though qualitative, gives a consistent explanation of the relatively simple properties of the two-pole cumulates.

6. Implication for the BKSK liquid line of descent

Accepting the 2-pole cumulate concept and the breakdown of the BKSK cumulates into three types (essentially leuconoritic, gabbronoritic and jotunitic cumulates), we can now investigate the relationship between cumulates and liquid line of descent (LLD), a major and classic issue in the study of layered intrusions. Fig. 11 schematically illustrates the theoretical relationship in a compositional plane between melts forming the LLD and cumulates. The early LLD is represented by two linear segments, L_1L_2 and L_2L_3, starting from L_1, the parental magma composition, and showing a sharp change in direction at L_2. The conjugated cumulate rocks, C_1 (pih-C) and C_2 (pihmac-C), representing cotectic assemblages in equilibrium with L_1 and L_2, respectively, are lying on their respective straight lines in keeping with the 2-pole cumulate concept. Note that C_1 and C_2 should theoretically lie on the tangents to the LLD at points L_1 and L_2, respectively, but here this precision is unnecessary because the LLD is simplified to straight lines.

In BKSK, the composition of the parental magma L_1 is reasonably well known (Wilson et al., 1996). The Tjörn jotunite (TJ) has been chosen here (Duchesne and Hertogen, 1988). It is a typically chilled rock close to the NW contact with surrounding gneisses, which has been experimentally shown to crystallize, at the 5 kbar liquidus, minerals close in composition to those observed in the primitive association of MCU III and IV (Vander Auwera and Longhi, 1994). The TJ composition is close to the Hidra marginal facies (Demaiffe and Hertogen, 1981; Duchesne et al., 1985) and to chilled margin sample B90 of Robins et al. (1997) from the basal contact at the northern margin of BKSK. The TJ composition has been called primitive jotunite by Vander Auwera

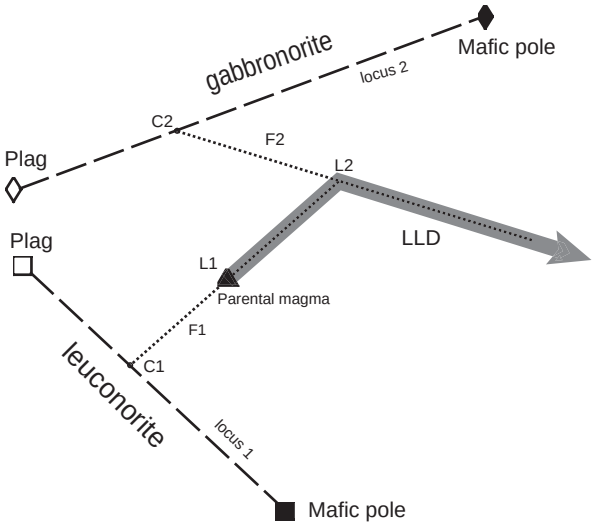

Fig. 11. Schematic representation of the cumulate–melt relationship in a three-component phase diagram/compositional plane. The LLD is illustrated by two linear segments. The cotectic cumulate compositions C_1 and C_2 lie on their respective tie lines joining the poles.

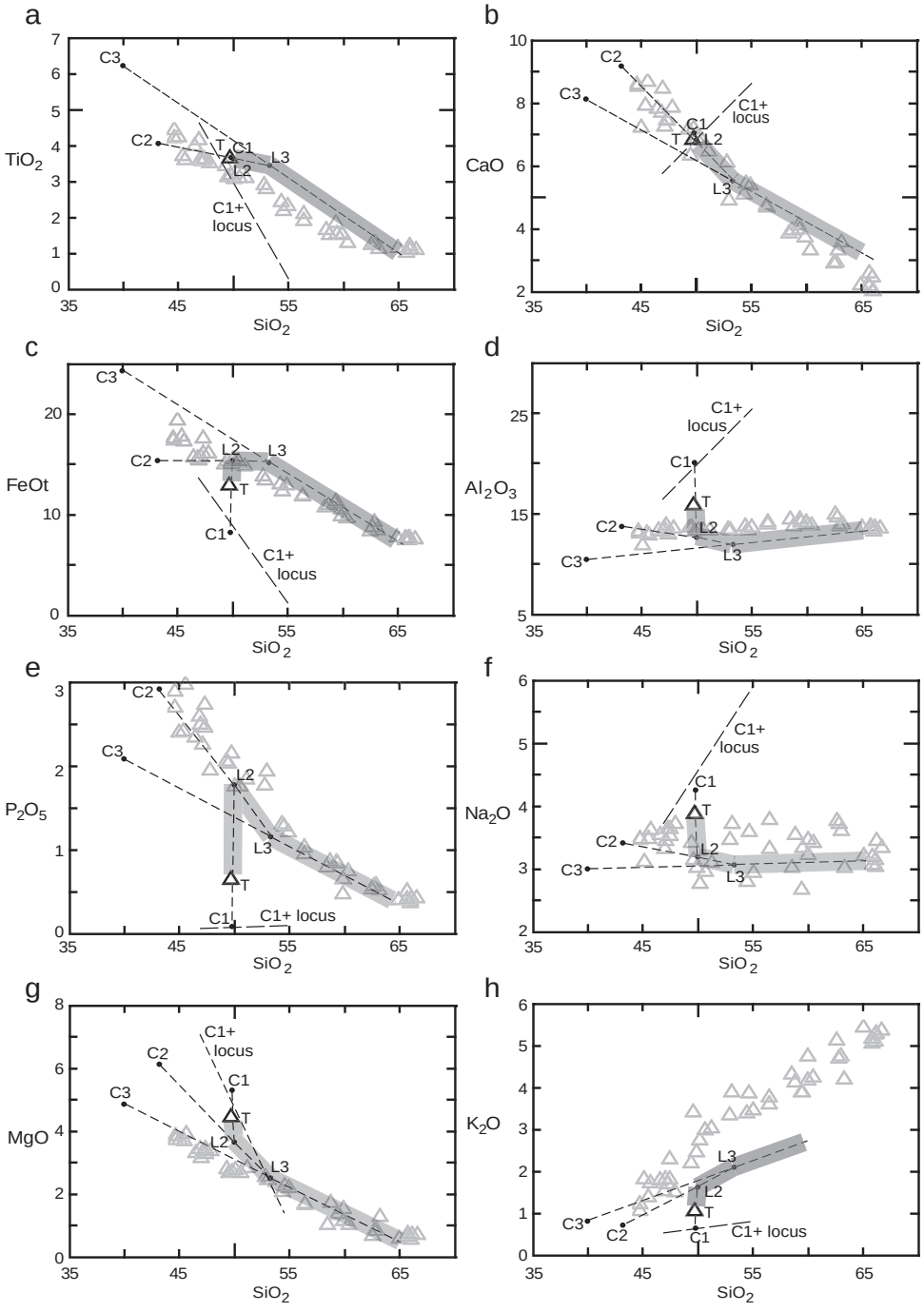

Fig. 12. (a to h) Harker diagrams showing the graphical reconstruction of the Bjerkreim–Sokndal LLD through a 3-stage mass-balance modelling. Legend: open triangle: Tjörn jotunitic parental magma; open grey triangles: samples defining the jotunite LLD (from Vander Auwera et al., 1998); long dashed line indicated C_{1+} locus: part of the straight line joining the magnetite–leuconorite mafic pole to the plagioclase pole.

et al. (1998) because it is the less evolved composition in the jotunite series of rocks.

Parts of the jotunitic LLD have already been assessed in Rogaland. The best constrained one, proposed by Vander Auwera et al. (1998), is based on samples from the Tellnes dyke (Wilmart et al., 1989) to which a series of dyke rocks with chilled textures has been added. It results from fractional crystallization of an evolved jotunite, sensu Vander Auwera et al. (1998) and extends to charnockite compositions. This LLD has furthermore been experimentally constrained (Vander Auwera and Longhi, 1994; Vander Auwera et al., 1998), and is considered by Duchesne and Wilmart (1997) to have produced olivine-bearing quartz mangerite and charnockite in the upper part of the BKSK intrusion.

6.1. Step by step reconstruction of the LLD

It emerges from Fig. 12a–b that the average ilmenite–leuconorite cumulate C_1 has the same CaO and TiO_2 composition as the parental magma TJ. This strongly suggests that C_1 indeed represents the ilmenite–leuconorite cotectic composition because the number of samples of that type ($n=43$) is large enough to guarantee a correct representation of the population. Accepting this hypothesis, we infer from Fig. 12a–b that subtraction of C_1 from TJ does not fractionate CaO and TiO_2 and that the resulting liquid L_2 has the same CaO and TiO_2 composition as C_1 and TJ. This imposes the SiO_2 value of L_2. Then, by trial and error, we have fixed the other element contents of L_2 as close as possible to the LLD (Fig. 12c–g). The result is displayed in Table 4. The fraction of liquid F left after this subtraction is somewhat variable from element to element, but considering the accuracy with which the LLD is defined, it can be estimated that a F value close to 0.6 (on the basis of the FeOt and Al_2O_3 diagrams, Fig. 12c–d) is acceptable, in agreement with the value (0.5) obtained by Vander Auwera et al. (1998), and an estimate of 0.47 calculated by modelling the Sr-content evolution of plagioclase (Duchesne, 1978).

Noting that the locus of the magnetite–leuconorite cumulate is passing very close to C_1 in all diagrams (Fig. 12), we postulate that the C_{1+} cotectic composition is identical "within errors" to C_1. This implies that the number of magnetite–leuconorite samples ($n=13$) is not large enough to be representative of the population. Subtraction of this C_{1+} will thus have a negligible effect on the evolution.

In a second step the average gabbronoritic cumulate C_2 is subtracted from L_2 and gives the L_3 melt composition (Table 4; Fig. 12). Again here we postulate that C_2 represents the gabbronorite cotectic composition because the number of samples of this type is large ($n=39$). It can be seen from the AFM projection (Fig. 13) that a third cumulate C_3 has to be subtracted from L_3 to better simulate the evolved part of the LLD. This cumulate C_3, called jotunitic cumulate, is made up of a ternary feldspar ($An_{32}Ab_{56}Or_{12}$) and a mafic pole intermediate between the gabbronoritic pole and the UML (Fig. 10; Table 4). The graphical expression of the modelling, shown in Figs. 12 and 13, can reasonably account for the evolution of the LLD. Note that the sum of the elements in the calculated compositions is close to 100% (Table 4), which is a good test of the validity of the approach.

6.2. The P_2O_5 problem

Our reconstruction of the LLD, however, fails to account for the P_2O_5 evolution in the first step of the calculation (Fig. 12e). It emerges from the graphical representation that the fraction of melt (F) left after

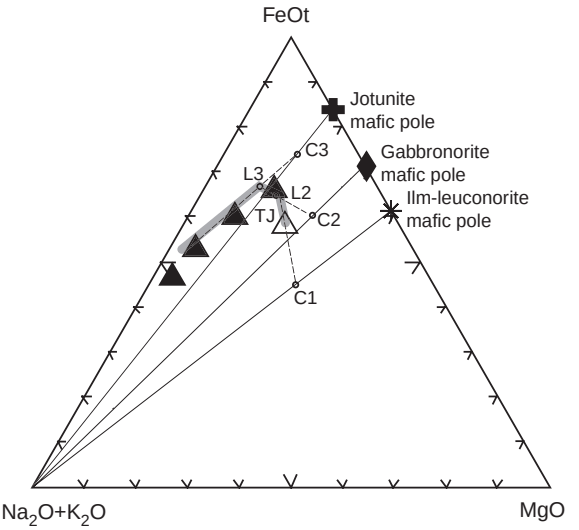

Fig. 13. AFM (Na_2O+K_2O–FeOt–MgO) projection of the 3-stage model. Legend: see Fig. 12 (filled triangles: representative samples of the LLD).

subtraction of C_1 has a value of 0.37, much lower than the value of F (ca 0.60) calculated with e.g. FeOt and Al_2O_3 (Fig. 12c–d). On the other hand, a value of 1% P_2O_5 in the parental magma would fit the observed LLD. We believe that the difference with the Tjörn value (0.64% P_2O_5) remains in the possible range of natural variation in primitive jotunite, and is thus not significant.

6.3. Evidence of contamination

The K_2O evolution also shows a major discrepancy (Fig. 12h): the calculated model strongly diverges from the LLD and is thus unable to account for the most evolved rocks of the intrusion. As we have seen, the K_2O content of the cumulates strongly depends on the amount of trapped liquid, so the average K_2O contents of the leuconoritic and gabbronoritic cumulates are higher than the values given by the 2-pole mixture. However, even in the most conservative situation, in which the C_1 cumulate value (0.25% K_2O) is chosen on the 2-pole mixing line and a value of $F=0.4$ is adopted, the model trend still diverges significantly from what is observed in the rocks. Two scenarios can explain this divergence: (1) similarly to the P_2O_5 case, the K_2O content of the parental magma might have been higher than the TJ value. To match the observed trend and the range of F values from 0.4 to 0.6, K_2O should vary from 1.3% to 1.6%. Values in this range have been reported by Robins et al. (1997) for marginal jotunites, but these rocks display much higher initial Sr isotopic ratios (0.708–0.714) than the Tjörn facies (0.704) (Bolle et al., 2003), possibly due to local contamination; (2) some K_2O has been added to the system during fractional crystallization because the system was open during differentiation. This finds support in the Sr isotopic composition which shows a steady increase through MCU IV from 0.705 to 0.7085 (Nielsen et al., 1996; Wilson et al., 1996). Occurrence in the uppermost acidic rocks of incompletely resorbed leucogranitic enclaves also suggests contamination by migmatitic leucosomes (Duchesne and Wilmart, 1997).

6.4. Implication for the formation of evolved jotunites

Comparison of the BKSK calculated LLD with the observed one, based on dyke rock compositions, further reveals an interesting feature concerning the link between primitive and evolved jotunites. The Harker diagrams show that the BKSK evolution from a parental magma with the composition of TJ (a primitive jotunite) bypasses the most Fe-, Ti-, P-enriched melts (representing evolved jotunites) of the LLD. This means that such evolved jotunites cannot be produced from primitive jotunites at the relatively low pressure of BKSK crystallization (ca. 5 kbar, Vander Auwera and Longhi, 1994). This corroborates a conclusion of Longhi et al. (1999), drawn from experimental data, in which higher pressures are needed to fractionate evolved jotunite from primitive jotunite. Indeed, at high pressure the liquidus plagioclase is more albitic and its subtraction can decrease the SiO_2 content of the melt.

6.5. Implications for anorthosite formation in MCU I

For reasons already mentioned above, samples from MCU IA and IB have not been considered in this survey. It is thus worth examining now to what extent this strategy could have biased the approach. Indeed, MCU IA is dominated by anorthositic cumulates (Fig. 5), which points to the possibility of a very first stage of crystallization in which plagioclase was the only liquidus phase.

Fig. 14 illustrates the evolution for CaO, a critical element in the modelling. We suppose that the subtracted liquidus plagioclase P_0 has an anorthite content of An_{47}, in the range of $An_{49–36}$ reported for MCU I cumulates by Wilson et al. (1996) and slightly more primitive than the plagioclase of the leuconorite cumulates (An_{45}). Because the parental magma composition TJ is close to the line C_3L_3 which simulates the evolved part of the LLD, the amounts of P_0 and C_2 that can be subtracted are very limited, and, grossly, the only effect on the LLD would be to curve the beginning of the trajectory. We can thus conclude that the amount of anorthosite produced in this scenario would be very small and would not basically modify the model presented in Fig. 12.

It therefore emerges that the amount of anorthosite in MCU IA is not accounted for by fractional crystallization of the Tjörn parental magma in the conditions prevailing in the BKSK magma chamber. A possible hypothesis would be that part of the plagioclase formed in a deeper magma chamber and

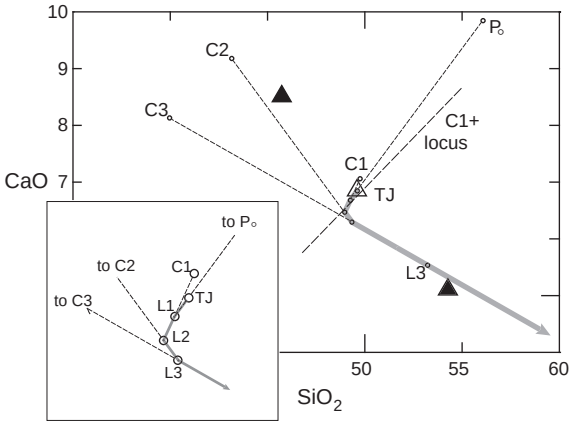

Fig. 14. CaO vs. SiO_2. Tentative illustration of the effect of subtracting an anorthositic cumulate (p-C), made up of plagioclase P_0 (An_{47}), before cumulate C_1. Due to the proximity of C_1 and TJ to C_3L_3, the amounts of P_0 and C_2 that can be subtracted are very small ($\approx$ 5% and $\approx$ 6%, respectively) and unrealistic. Note that the C_{1+} locus passes very close to L_1, and its subtraction has thus a negligible influence on the evolution. Inset focuses on the early part of the LLD. Filled triangles: representative samples of the LLD.

was brought into the BKSK chamber as phenocrysts in the first influx of magma. An alternative hypothesis would be to suppose a different composition for the parental magma of MCU IA and IB. Wilson et al. (1996) have indeed noted that the sequence in which cumulus minerals occur in MCU IA and IB slightly differs from the later MCU. These hypotheses need further investigation.

7. Implications for the cryptic layering of mafic minerals

It has been shown that the leuconorite and gabbronorite mafic poles have constant compositions in the Layered Series. This property, illustrated in the AFM projection (Fig. 13), has already been mentioned for the ultramafic rocks (UML) of the Transition Zone (Duchesne et al., 1987). Fig. 13 shows that the Mg# of a given mafic pole is constant during the whole interval of crystallization of this type of cumulate, and particularly for the jotunite mafic pole. Actually, cryptic layering is conspicuous in all mafic phases and the Mg# of the pyroxenes and of the olivine changes significantly, together with the oxide mineral compositions. For example, in gabbronoritic cumulates, the Mg# of Ca-poor pyroxene distinctly decreases from 0.67 to 0.55 (Wilson et al., 1996), the hematite content of the ilmenite solid solution decreases from 9% Hem to 3% Hem, and the TiO_2 content of magnetite increases from 4% to 8% (Duchesne, 1972a). Similarly, in the UML, the olivine composition varies from Fo_{30} to Fo_{19} and the magnetite from 15% to 19% TiO_2 (Duchesne et al., 1987). Amazingly the increase in FeOt in the ferromagnesian minerals is exactly balanced by the decrease of FeOt in the Fe–Ti oxides in order to maintain a constant bulk Mg# value. This buffering effect has never, to the authors' knowledge, been noticed in magmatic series, though in AFM diagrams linear trends (towards the A corner and with constant FeOt/MgO ratio), classically called Fenner trends, are a straightforward illustration of this effect: the Fe/Mg ratio remains constant though the various minerals change in composition and show cryptic layering. What we observed here is a mere illustration of this effect.

8. Conclusions

1. Three types of cumulates can be distinguished in the 3 uppermost megacyclic units in the Bjerkreim–Sokndal layered intrusion on the basis of whole-rock major element composition. They correspond to the three major types of cumulates, i.e. ilmenite–leuconorite (phi-C), magnetite–leuconorite (phim-C) and gabbronorite (phimac-C).
2. For a given cumulate type, no difference in whole-rock major element composition can be detected from MCU II to MCU IV, which points to insignificant compositional difference in the successive magma influxes.
3. For each cumulate type, linear trends in Harker diagrams reflect a mixing relationship between a plagioclase pole and a mafic pole comprising all the mafic minerals, the trapped liquid fraction having a second order influence (adcumulates to mesocumulates). The mafic pole remains remarkably constant for a given type of cumulate even though the various minerals constituting the pole vary in composition (cryptic layering).

4. In the mafic poles, the constant proportions of mafic minerals with contrasting densities (thus most likely to be sorted by gravity-controlled processes of formation) preclude accumulation by gravity.
5. For similar reasons, formation of an Fe–Ti-rich immiscible liquid during crystallization can be excluded.
6. The absence of accumulation evidence implies that a model of in situ crystallization, already proposed by Vander Auwera and Longhi (1994) for plagioclase, can be extended to the mafic minerals. It therefore emerges that variations in plagioclase modal contents are due to variations in plagioclase nucleation rate.
7. The characteristic properties of the 2-pole cumulate suggest a crystallization process in magma layers formed by double-diffusive processes. The nucleation rate of the plagioclase would be controlled by the cooling regime and self-nucleation.
8. The 2-pole cumulate concept can be applied to more than 90% of the investigated layered series, but it is by no means universal since the Transition Zone cumulates show evidence of mineral sorting during crystallization.
9. Accepting the Tjörn jotunite of Duchesne and Hertogen (1988) and Vander Auwera and Longhi (1994) as the parental magma, and the LLD of Vander Auwera et al. (1998) as describing the melt evolution, modelling of the cumulate/melt relationships by graphical methods gives a consistent view which confirms that:
   - cotectic compositions can be represented by average cumulate compositions provided the number of samples is large;
   - cumulates and related melt compositions from MCU II to MCU IV can be accounted for by the model;
   - a K_2O contaminant must be involved in the formation of the acidic rocks of the upper part of the intrusion, in agreement with isotope data of Nielsen et al. (1996);
   - the large volume of anorthosite in MCU I cannot be accounted for, which implies a different parental magma for MCU I or different crystallization conditions than those prevailing in the BKSK magma chamber;
   - evolved jotunite (Fe-, Ti-, and P-rich melt) cannot be produced by crystallization of primitive jotunites at the final depth of emplacement of anorthosites (3–5 kbar).
10. The mafic mineral compositional variations (cryptic layering) are buffered by the balanced evolution of ferromagnesian minerals and Fe–Ti oxides. This effect can explain linear trends of evolution in AFM diagrams (Fenner trends).

Acknowledgements

The authors particularly thank A. Albert for performing the statistical analysis. G. Bologne helped with the XRF analyses and performed the wet chemical analyses. I. Roelandts supervised the wet chemical laboratory in the 1963–1972 period. J. Michot has contributed to establishing of the Paul Michot database. J. Vander Auwera, R.G. Cawthorn and R.A. Wiebe are thanked for their encouraging discussions. The constructive reviews of J. Bédart and J.R. Wilson were greatly appreciated. This work was supported by the Belgian Fund for Joint Research. The Fund for Research in Industry and Agriculture (FRIA) provided a grant to BC.

Appendix A

The 57 rocks from the Paul Michot collection were analysed by wet chemistry in the period 1964–1972 by G. Bologne and I. Roelandts. The method was derived from that of Shapiro and Brannock (1962) with considerable improvements (e.g. SiO_2 was measured by gravity, CaO and MgO were measured by EDTA after extraction by $CHCl_3$). International standard rocks, including G-1 and W-1, were used to assess the accuracy of the method (Roelandts and Duchesne, 1968); 23 samples collected by J.C. Duchesne were analysed by G. Bologne and J.C. Duchesne by XRF in the period 1975–1995, using a CGR Lamda 2020 semi-automatic spectrometer and following the method of Norrish and Hutton (1969); accuracy and reproducibility were evaluated on the basis of a collection of international standards (Bologne and Duchesne, 1991); 9 samples collected by the authors were analysed by XRF in 2000 using

an ARL 9800 XP automatic spectrometer on Li-borate glass; matrix corrections were determined using a set of 46 international standards. The nine samples from Jensen et al. (2003) were analysed by XRF at the University of Aarhus.

References

Barling, J., Weis, D., Demaiffe, D., 2000. A Sr-, Nd-, and Pb-isotopic investigation of the transition between two megacyclic units of the Bjerkreim–Sokndal layered intrusion, south Norway. Chem. Geol. 165, 47–65.

Bédard, J.H., 1994. A procedure for calculating the equilibrium distribution of trace elements among the minerals of cumulate rocks, and the concentrations of trace elements in the coexisting liquids. Chem. Geol. 118, 143–153.

Bolle, O., Diot, H., Duchesne, J.C., 2000. Magnetic fabric and deformation in charnockitic igneous rocks of the Bjerkreim–Sokndal layered intrusion (Rogaland, Southwest Norway). J. Struct. Geol. 22, 647–667.

Bolle, O., Trindade, R.I.F., Bouchez, J.L., Duchesne, J.C., 2002. Imaging downward granitic magma transport in the Rogaland Igneous Complex. Terra Nova 14, 87–92.

Bolle, O., Demaiffe, D., Duchesne, J.C., 2003. Petrogenesis of jotunitic and acidic members of an AMC suite (Rogaland anorthosite province, SW Norway): a Sr and Nd isotopic assessment. Precambrian Res. 124, 185–214.

Bologne, G., Duchesne, J.C., 1991. Analyse des roches silicatées par spectrométrie de fluorescence X: précision et exactitude. Prof. Paper-Geol. Surv. Belg. 249, 1–11.

Bowen, N.L., 1928. The Evolution of the Igneous Rocks. Princeton University Press, Princeton. 334 pp.

Brandeis, G., Jaupart, C., 1987. Characteristic dimensions and times for dynamic crystallization. In: Parsons, I. (Ed.), Origins of Igneous Layering. Reidel, Dordrecht, pp. 613–640.

Campbell, I.H., 1978. Some problems with the cumulus theory. Lithos 11, 311–323.

Campbell, I.H., Roeder, P.L., Dixon, J.M., 1978. Plagioclase buoyancy in basaltic liquids as determined with a centrifuge furnace. Contrib. Mineral. Petrol. 67, 369–377.

Cawthorn, R.G., 1996. Layered Igneous Rocks. Development in Petrology. Elsevier, Amsterdam. 531 pp.

Charlier, B., Vander Auwera, J., Duchesne, J.C., 2005. Geochemistry of cumulates from the Bjerkreim–Sokndal layered intrusion (S. Norway): Part II. REE and the trapped liquid fraction. Lithos 83, 255–276 (this issue).

Davis, J.C., 1986. Statistics and Data Analysis in Geology, 2nd edition. John Wiley, New York. 550 pp.

Deer, W.A., Howie, R.A., Zussman, J., 1966. An Introduction to Rock-Forming Minerals. Longmans, London. 528 pp.

Demaiffe, D., Hertogen, J., 1981. Rare earth element geochemistry and strontium isotopic composition of a massif-type anorthositic-charnockitic body: the Hidra massif (Rogaland, S.W. Norway). Geochim. Cosmochim. Acta 45, 1545–1561.

Duchesne, J.C., 1972a. Iron–titanium oxide minerals in the Bjerkrem-Sogndal massif, South-Western Norway). J. Petrol. 13, 57–81.

Duchesne, J.C., 1972b. Pyroxènes et olivine dans le massif de Bjerkrem-Sogndal (Norvège méridionale). Contribution à l'étude de la série anorthosite–mangérite, 24ème Congrès Géologique International, Montréal, pp. 320–328.

Duchesne, J.C., 1978. Quantitative modeling of Sr, Ca, Rb and K in the Bjerkrem-Sogndal layered lopolith (S.W. Norway). Contrib. Mineral. Petrol. 66, 175–184.

Duchesne, J.C., 1996. Liquid ilmenite or liquidus ilmenite: a comment on the nature of ilmenite vein deposit. In: Demaiffe, D. (Ed.), Petrology and Geochemistry of Magmatic Suites of Rocks in the Continental and Oceanic Crusts. ULB-MRAC, Bruxelles, pp. 73–82.

Duchesne, J.C., 2001. The Rogaland Intrusive Massifs—an excursion guide. NGU reports 2001.29. NGU Report 2001.29, Geological Survey of Norway. 139 pp.

Duchesne, J.C., Hertogen, J., 1988. Le magma parental du lopolithe de Bjerkreim–Sokndal (Norvège méridionale). C.R. Acad. Sci. Paris 306, 45–48.

Duchesne, J.C., Wilmart, E., 1997. Igneous charnockites and related rocks from the Bjerkreim–Sokndal layered intrusion (Southwest Norway): a jotunite (hypersthene monzodiorite)-derived A-type granitoid suite. J. Petrol. 38 (3), 337–369.

Duchesne, J.C., Demaiffe, D., Roelandts, I., Weis, D., 1985. Petrogenesis of monzonoritic dykes in the Egersund-Ogna anorthosite (Rogaland, S.W. Norway): trace elements and isotopic constraints. Contrib. Mineral. Petrol. 90, 214–225.

Duchesne, J.C., Denoiseux, B., Hertogen, J., 1987. The norite–mangerite relationships in the Bjerkreim–Sokndal layered lopolith (SW Norway). Lithos 20, 1–17.

Duchesne, J.C., Wilmart, E., Demaiffe, D., Hertogen, J., 1989. Monzonorites from Rogaland (Southwest Norway): a series of rocks coeval but not comagmatic with massif-type anorthosites. Precambrian Res. 45, 111–128.

Duchesne, J.C., Liégeois, J.P., Vander Auwera, J., Longhi, J., 1999. The crustal tongue melting model and the origin of massive anorthosites. Terra Nova 11, 100–105.

Force, E.R., 1991. Geology of titanium mineral deposits. Spec. Pap.-Geol. Soc. Am. 259, 1–112.

Greer, A.L., Herlach, D.M., Kelton, K.F. (Eds.), Nucleation control, Philosophical Transactions of the Royal Society of London, vol. 361. London, 230 pp.

Henderson, P., 1968. The distribution of phosphorus in the early and middle stages of fractionation of some basic layered intrusions. Geochim. Cosmochim. Acta 32, 897–911.

Hort, M., Marsh, B.D., Spohn, T., 1993. Igneous layering through oscillatory nucleation and crystal settling in well-mixed magmas. Contrib. Mineral. Petrol. 114, 425–440.

Hosmer, D.W., Lemeshow, S., 1989. Applied Logistic Regression. John Wiley, New York.

Irvine, T.N., 1980. Magmatic infiltration metasomatism, double-diffusive fractional crystallization, and adcumulus growth in the Muskox intrusion and other layered intrusions. In: Hargraves, R.B. (Ed.), Physics of Magmatic Processes. Princeton University Press, Princeton, pp. 325–384.

Irvine, T.N., 1982. Terminology of layered intrusions. J. Petrol. 23, 127–162.

Jensen, J.C., Nielsen, F.M., Duchesne, J.C., Demaiffe, D., Wilson, J.R., 1993. Magma influx and mixing in the Bjerkreim–Sokndal layered intrusion, South Norway: evidence from the boundary between two megacyclic units at Storeknuten. Lithos 29, 311–325.

Jensen, K., Wilson, J.R., Robins, B., Chiodoni, F., 2003. A sulphide-bearing orthopyroxenite layer in the Bjerkreim–Sokndal Intrusion: implications for processes during magma-chamber replenishment. Lithos 67, 15–37.

Longhi, J., Vander Auwera, J., Fram, M., Duchesne, J.C., 1999. Some phase equilibrium constraints on the origin of Proterozoic (Massif) anorthosites and related rocks. J. Petrol. 40 (2), 339–362.

Maaløe, S., 1978. The origin of rhythmic layering. Mineral. Mag. 42, 337–345.

Maier, W.D., Barnes, S.-J., 1998. Concentrations of rare earth elements in silicate rocks of the Lower, Critical and Main Zones of the Bushveld intrusion. Chem. Geol. 150, 85–103.

Marker, M., Schiellerup, H., Meyer, G.B., Robins, B., Bolle, O., 2003. Geological map of the Rogaland anorthosite Province (at scale 1:75,000). In: Duchesne, J.C., Korneliussen, A. (Eds.), Ilmenite Deposits and Their Geological Environments. Norges geologiske undersøkelse, Trondheim.

McBirney, A.R., Noyes, R.M., 1979. Crystallization and layering of the Skaergaard intrusion. J. Petrol. 20, 487–554.

Michot, P., 1960. La géologie de la catazone: le problème des anorthosites, la palingenèse basique et la tectonique catazonale dans le rogaland méridional (Norvège méridionale). Norges Geol. Unders. 212g, 1–54.

Michot, P., 1965. Le magma plagioclasique. Geol. Rundsch. 54, 956–976.

Morse, S.A., 1979. Kiglapait geochemistry: I. Systematics, sampling, and density. J. Petrol. 20 (3), 555–590.

Morse, S.A., 1981. Kiglapait geochemistry: IV. The major elements. Geochim. Cosmochim. Acta 45, 461–473.

Nielsen, F.M., Wilson, J.R., 1991. Crystallization processes in the Bjerkreim-Sokndal layered intrusion, south Norway: evidence from the boundary between two macrocyclic units. Contrib. Mineral. Petrol. 107, 403–414.

Nielsen, F.M., Campbell, I.H., McCulloch, M., Wilson, J.R., 1996. A strontium isotopic investigation of the Bjerkreim–Sokndal layered intrusion, southwest Norway. J. Petrol. 37, 171–193.

Norrish, K., Hutton, J.T., 1969. An accurate X-ray spectrographic method for the analysis of a wide range of geological samples. Geochim. Cosmochim. Acta 33, 431–453.

Paludan, J., Hansen, U.B., Olesen, N.Ø., 1994. Structural evolution of the Precambrian Bjerkreim–Sokndal intrusion, South Norway. Norsk Geolog. Tidsskr. 74, 185–198.

Parsons, I. (Ed.), Origins of Igneous Layering, NATO ASI series, vol. C196. Reidel, Dordrecht. 666 pp.

Philpotts, A.R., 1981. A model for the generation of massif-type anorthosites. Can. Mineral. 19, 233–253.

Robins, B., Tumyr, O., Tysseland, M., Garmann, L.B., 1997. The Bjerkreim–Sokndal Layered Intrusion, Rogaland, S.W. Norway: evidence from marginal rocks for a jotunite parent magma. Lithos 39, 121–133.

Roelandts, I., Duchesne, J.C., 1968. Méthodes d'analyse des roches silicatées. Principe et discussion de la précision et de l'exactitude obtenues. Ann. Soc. Géol. Belg. 91, 159–164.

Schärer, U., Wilmart, E., Duchesne, J.C., 1996. The short duration and anorogenic character of anorthosite magmatism: U–Pb dating of the Rogaland complex, Norway. Earth Planet. Sci. Lett. 139, 335–350.

Sparks, R.S.J., Huppert, H.E., Kerr, R.C., McKenzie, D.P., Tait, S.R., 1985. Postcumulus processes in layered intrusions. Geol. Mag. 122, 555–568.

Vander Auwera, J., Longhi, J., 1994. Experimental study of a jotunite (hypersthene monzodiorite): constraints on the parent magma composition and crystallization conditions (P, T, fO_2) of the Bjerkreim–Sokndal layered intrusion. Contrib. Miner. Petrol. 118, 60–78.

Vander Auwera, J., Longhi, J., Duchesne, J.C., 1998. A liquid line of descent of the jotunite (hypersthene monzodiorite) suite. J. Petrol. 39, 439–468.

Wager, L.R., Brown, G.M., 1968. Layered Igneous Rocks. Oliver and Boyd Ltd., Londres. 588 pp.

Wilmart, E., Demaiffe, D., Duchesne, J.C., 1989. Geochemical constraints on the genesis of the Tellnes ilmenite deposit (S.W. Norway). Econ. Geol. 84, 1047–1056.

Wilson, J.R., Robins, B., Nielsen, F., Duchesne, J.C., Vander Auwera, J., 1996. The Bjerkreim–Sokndal layered intrusion, Southwest Norway. In: Cawthorn, R.G (Ed.), Layered Intrusions. Elsevier, Amsterdam, pp. 231–256.